

University of Nebraska - Lincoln

DigitalCommons@University of Nebraska - Lincoln

Biochemistry -- Faculty Publications

Biochemistry, Department of

Integrative computational approach identifies drug targets in CD4+ T-cell-mediated immune disorders

Bhanwar L. Puniya

Rada Amin

Bailee Lichter

Robert Moore

Alex Ciurej

See next page for additional authors

Follow this and additional works at: <https://digitalcommons.unl.edu/biochemfacpub>



Part of the [Biochemistry Commons](#), [Biotechnology Commons](#), and the [Other Biochemistry, Biophysics, and Structural Biology Commons](#)

This Article is brought to you for free and open access by the Biochemistry, Department of at DigitalCommons@University of Nebraska - Lincoln. It has been accepted for inclusion in Biochemistry -- Faculty Publications by an authorized administrator of DigitalCommons@University of Nebraska - Lincoln.

Authors

Bhanwar L. Puniya, Rada Amin, Bailee Lichter, Robert Moore, Alex Ciurej, Sydney J. Bennett, Ab Rauf Shah, Matteo Barberis, and Tomáš Helikar

ARTICLE OPEN



Integrative computational approach identifies drug targets in CD4⁺ T-cell-mediated immune disorders

Bhanwar Lal Puniya¹, Rada Amin¹, Bailee Lichter^{1,5}, Robert Moore^{1,5}, Alex Ciurej¹, Sydney J. Bennett¹, Ab Rauf Shah¹, Matteo Barberis^{2,3,4} and Tomáš Helikar¹

CD4⁺ T cells provide adaptive immunity against pathogens and abnormal cells, and they are also associated with various immune-related diseases. CD4⁺ T cells' metabolism is dysregulated in these pathologies and represents an opportunity for drug discovery and development. Genome-scale metabolic modeling offers an opportunity to accelerate drug discovery by providing high-quality information about possible target space in the context of a modeled disease. Here, we develop genome-scale models of naïve, Th1, Th2, and Th17 CD4⁺ T-cell subtypes to map metabolic perturbations in rheumatoid arthritis, multiple sclerosis, and primary biliary cholangitis. We subjected these models to *in silico* simulations for drug response analysis of existing FDA-approved drugs and compounds. Integration of disease-specific differentially expressed genes with altered reactions in response to metabolic perturbations identified 68 drug targets for the three autoimmune diseases. *In vitro* experimental validation, together with literature-based evidence, showed that modulation of fifty percent of identified drug targets suppressed CD4⁺ T cells, further increasing their potential impact as therapeutic interventions. Our approach can be generalized in the context of other diseases, and the metabolic models can be further used to dissect CD4⁺ T-cell metabolism.

npj Systems Biology and Applications (2021)7:4; <https://doi.org/10.1038/s41540-020-00165-3>

INTRODUCTION

CD4⁺ T cells are essential components of the human immune system that fight against pathogenic invaders and abnormal cells by producing cytokines and stimulating other cells, such as B cells, macrophages, and neutrophils¹. During an immune response, CD4⁺ T cells are activated and proliferate, and their metabolism adjusts to fulfill increased bioenergetic and biosynthetic demands. For example, activated effector CD4⁺ T cells are highly glycolytic² and use aerobic glycolysis and oxidative phosphorylation (OXPHOS) for proliferation³. On the other hand, naïve, resting, and regulatory CD4⁺ T cells are less glycolytic and use OXPHOS and fatty acid oxidation (FAO) for energy generation. Accordingly, metabolically dysregulated CD4⁺ T cells were observed in several diseases such as diabetes⁴, atherosclerosis⁵, cancers⁶, and autoimmune diseases such as rheumatoid arthritis (RA)^{7,8}, multiple sclerosis (MS)⁹, primary biliary cholangitis (PBC)¹⁰, and systemic lupus erythematosus (SLE)^{11,12}. Furthermore, metabolism of Type 1 T helper (Th1), Type 17 T helper (Th17), and inducible regulatory T cells have been found to be dysregulated in MS¹³. Controlling CD4⁺ metabolic pathways can be important in fighting against some immune diseases. For example, CD4⁺ T cells are hyperactive in systemic lupus erythematosus (SLE), and inhibiting glycolysis as well as the mitochondrial metabolism improved the outcome in an animal model¹⁴. Together, this evidence suggests a significant role of CD4⁺ T-cell metabolism in immune-mediated diseases.

Repurposing existing drugs for novel indications represents a cost-effective approach for the development of new treatment options¹⁵. Several studies have recently demonstrated the potential for drug repurposing in CD4⁺ T-cell-mediated diseases^{16,17}. For example, 2-deoxy-D-glucose (anticancer agent) and metformin (antidiabetic drug) were shown to reverse SLE in a

mouse model¹⁴. However, drug repurposing, as well as drug discovery and development efforts for targeting T-cell metabolism, have been limited due to the lack of knowledge about the key molecular targets in this context.

In recent years, analysis of large-scale biological datasets has emerged as a powerful strategy for discovering novel mechanisms, drug targets, and biomarkers in human diseases^{18–21}. Here, we develop a computational modeling approach that integrates multi-omic data with systematic perturbation analyses of newly constructed whole-genome metabolic models of naïve CD4⁺ T cells and Th1, Th2, and Th17 cells. This led to identifying potential drug targets for CD4⁺ T-cell-mediated diseases (RA, MS, and PBC).

RESULTS

Identification of genes expressed in the CD4⁺ T cells

We used the computational approach shown in Fig. 1 (see also Supplementary Methods 1) to construct metabolic models of naïve and effector CD4⁺ T cells. To identify metabolic genes expressed across CD4⁺ T-cell subtypes (naïve, Th1, Th2, and Th17 cells), we integrated transcriptomics^{22–30} and proteomics data³¹ (see Materials and methods; Supplementary Data 1). The comparison of genes expressed in CD4⁺ T-cell subtypes identified by different datasets is shown in Supplementary Fig. 1. The analysis showed that between 675 and 836 metabolic genes were expressed depending on the CD4⁺ T-cell subtype (Supplementary Data 2). Of these, 530 genes were expressed in all subtypes (Fig. 2a). On the other hand, 16, 25, 7, and 96 genes were specific to naïve, Th1, Th2, and Th17 cells, respectively. Pathway enrichment analysis using expressed metabolic genes suggested 6 enriched

¹Department of Biochemistry, University of Nebraska-Lincoln, Lincoln, USA. ²Systems Biology, School of Biosciences and Medicine, Faculty of Health and Medical Sciences, University of Surrey, Guildford, UK. ³Centre for Mathematical and Computational Biology, CMCB, University of Surrey, Guildford, UK. ⁴Synthetic Systems Biology and Nuclear Organization, Swammerdam Institute for Life Sciences, University of Amsterdam, Amsterdam, The Netherlands. ⁵These authors contributed equally: Bailee Lichter, Robert Moore. ✉email: m.barberis@surrey.ac.uk; thelikar2@unl.edu

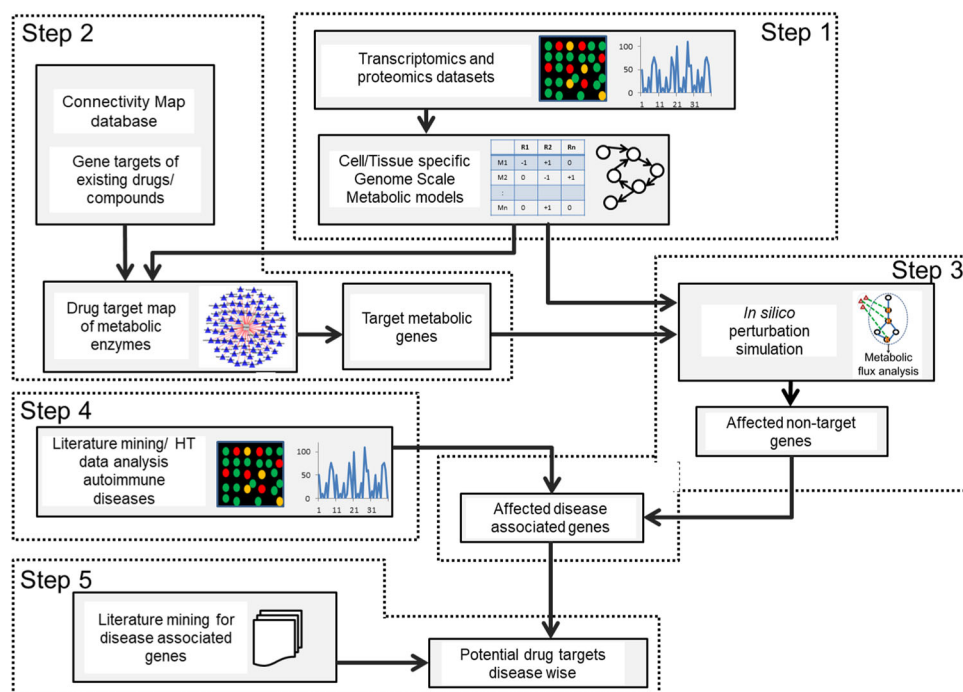


Fig. 1 Integrative approach for the identification of potential metabolic drug targets. The computational approach comprised of five major steps: (1) Construction of metabolic models using integrated transcriptomics and proteomics data, (2) Identification of metabolic genes that are targets for existing drugs/compounds, (3) In silico inhibition of targets of existing drugs to identify affected reactions, (4) Identification of differentially expressed genes (DEGs) in autoimmune diseases and their integration with flux ratios ($\text{Flux}_{\text{perturbed}} / \text{Flux}_{\text{WT}}$), and (5) Validation with literature and prediction of new targets.

KEGG pathways common across all subtypes: carbon metabolism, TCA cycle, oxidative phosphorylation (OXPHOS), amino sugar and nucleotide sugar metabolism, and valine, leucine, and isoleucine degradation (Fig. 2b). Fatty acid degradation and pentose phosphate pathway were enriched in naïve CD4^+ T cells only, and fatty acid metabolism was enriched in the naïve, Th2, and Th17 subtypes. No specific KEGG pathways were found enriched solely in Th1 and Th17 cells. Among the enriched pathways shared by all CD4^+ T cells, the TCA cycle was enriched more than two-fold in naïve, Th1, and Th2 subtypes. Similarly, OXPHOS was enriched more than two-fold in naïve and Th1 subtypes (Fig. 2c). These results suggest that key metabolic pathways are active across all the subtypes. Importantly, the metabolism of various CD4^+ T-cell subtypes can be different with respect to these pathways' levels of activity and the number of reactions active within the pathways.

Development and validation of genome-scale metabolic models of CD4^+ T cells

To further examine these issues, we developed constraint-based metabolic models specific to naïve CD4^+ T cells, Th1, Th2, and Th17 cells. Genome-scale constraint-based metabolic models include a structural representation of a cell's entire biochemical reactions and help in computing biochemically feasible functional states³². These models consist of a stoichiometry matrix of biochemical reactions, exchange reactions (connecting cells internal metabolism with the environment), and additional constraints for upper and lower bounds for fluxes to be identified. Using modeling approaches such as Flux Balance Analysis, these models can be solved to predict flux distribution. In addition to identifying feasible flux distribution, the constraint-based models are useful in understanding human disease and identifying drug targets, modeling interspecies interactions, and metabolic analysis of across strains and species³³. Our genome-scale metabolic models consist of 3956 to 5282 reactions associated with 1055 to 1250 genes (Supplementary Table 1; Supplementary Data 3–6).

The number of internal enzyme-catalyzed reactions was 2501, 1969, 2549, and 2640 for naïve, Th1, Th2, and Th17 models, respectively, distributed across 84 metabolic pathways (Supplementary Fig. 2; note that transport and exchange reactions were excluded). The models include more genes associations than expressed genes identified from the data because the model-building algorithm inserts some reactions that are not supported by data but required for the model to achieve essential metabolic functions for biomass production (see Materials and methods). Furthermore, the algorithm kept the complete gene rules associated with reactions catalyzed by multiple isozymes if one of them was expressed in the data. Thus, the final models comprise ~30% more genes than found in the data. Removing the unexpressed genes would not delete the model's reaction because the data support at least one isozyme. We compared our models with an existing model for naïve CD4^+ T cell (CD4T1670^{34}) (Supplementary Table 1). Since our models exclude blocked reactions and dead ends, we have removed dead ends from CD4T1670 for fair comparisons. Since we based all models of this study on the more recent human metabolic network Recon3D³⁵, they include more reactions and metabolites than CD4T1670 , based on Recon2³⁶.

We validated the models based on the active pathways and gene essentiality. We first identified pathways that are known to be active in different CD4^+ T-cell subtypes (see Materials and methods) and searched for their activity (with non-zero fluxes) in the corresponding models through Flux Balance Analysis (FBA). Several major pathways were in agreement with the literature. These include glycolysis, TCA cycle, glutaminolysis, and pyruvate to lactate conversion (aerobic glycolysis) that showed non-zero flux in all the models. We present an illustrative flux map of the pathways mentioned above for the naïve model in Fig. 3. The figure also indicates flux differences with the Th1 model for critical reactions. Flux maps for the Th1, Th2, and Th17 models are shown in Supplementary Figs. 3–5. Furthermore, we show some specific

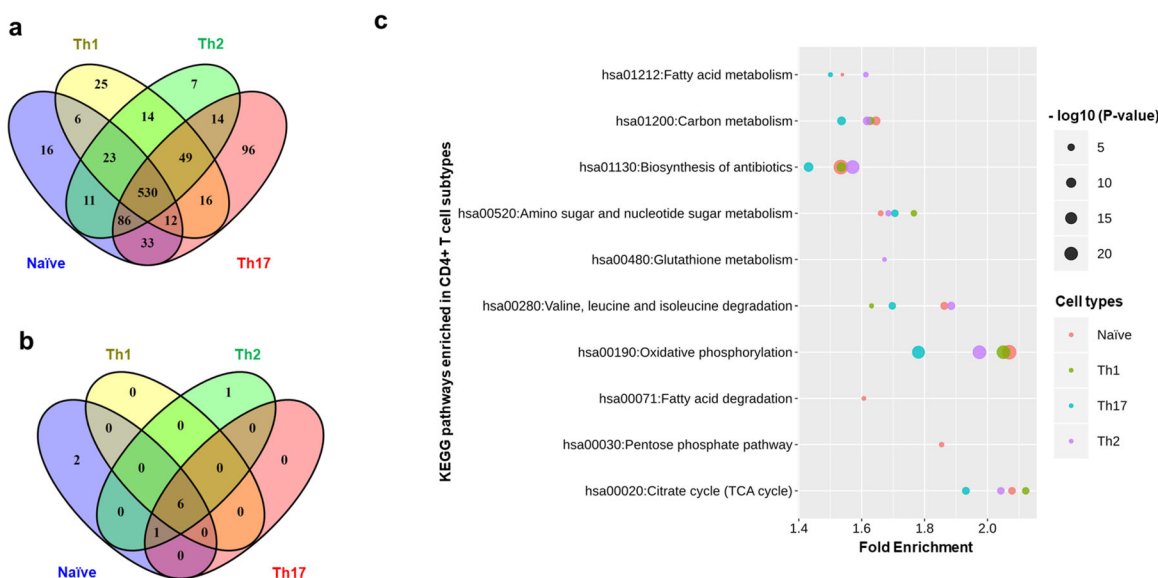


Fig. 2 Construction of metabolic models in CD4⁺ T cells. **a** Expressed metabolic genes identified using integrated transcriptomics and proteomics data of CD4⁺ T-cell subtypes. **b** KEGG pathway enrichment analysis of expressed genes in each cell type using all 1892 metabolic genes as a background. **c** Fold enrichment and *P*-values (larger sizes correspond to lower *P*-values) of KEGG pathways enriched across CD4⁺ T-cell subtypes. A pathway was considered significantly enriched with *P*-value < 0.05 and false discovery rate (FDR) < 5%.

observed behaviors of CD4⁺ T cells collected from the literature used for validation in Table 1. For comparison, we also performed these validations in CD4T1670, also shown in Table 1. In all the models developed in this study, limiting glucose from the environment resulted in a decreased growth rate (Fig. 4a), which is in agreement with existing knowledge^{37,38} but not reproduced by the CD4T1670 model (Supplementary Fig. 6). All our models produced lactate³⁹ (Table 1, Supplementary Fig. 7). Literature shows that increasing PDHm (pyruvate dehydrogenase) by inhibiting PDHK (pyruvate dehydrogenase kinase) would redirect flux from pyruvate to TCA cycle and, therefore, will decrease the lactate production³⁸. This was reproduced by our models (Fig. 4b). Our models were also able to reproduce the essentiality of Leucine, Arginine, and ACC1 for T-cell growth (Table 1), in agreement with the literature³⁸. It is important to note that the activity of some pathways in the models was not agreeing or partially agreeing with the literature. Specifically, we did not observe a significant effect on growth rate when glutamine⁴⁰ was removed from exchange reactions in the effector CD4⁺ T-cell models (Fig. 4c). However, literature has shown that while transporters of glutamine in activated CD4⁺ T cells are dispensable, removal of glutamine is critical and affects growth³⁸. Our systematic analyses showed that (1) inhibiting glutamine synthase (GLNS) (that converts glutamate to glutamine) in the absence of glutamine uptake in the model decreases growth to zero, and (2) glutamine can have an impact on growth when glucose availability is limited (less than 2 mmol/g.DW/hr) (Fig. 4d). Using CD4T1670, we observed no effect on biomass when varying glutamine in the presence and absence of glucose (Supplementary Fig. 8). Thus, we may hypothesize that glutamine might be conditionally critical for CD4⁺ T cells specifically when the availability of other nutrients is low.

Next, we predicted essential genes and compared the results against independent data to identify the overlap between genes predicted by our models and identified from experiments. Because large-scale essentiality datasets were not available for CD4⁺ T cells, we used essentiality datasets available for different human cancer cell lines. Gene deletion analysis predicted 84, 95, 81, and 84 genes as essential in the naïve, Th1, Th2, and Th17 models, respectively (Supplementary Data 7). More than 70% of these predictions agreed with genes experimentally defined as

essential and conditionally essential in those different but related cell lines⁴¹ (Supplementary Fig. 9). To assess if higher-ranked predictions compared better with gene essentiality data, we generated precision-recall curves using 84, 95, 81, and 84 genes, respectively, from each model that were identified as essential. The area under the curve for all models was >75% (Supplementary Figs. 10–13). Additional validations based on CD4⁺ T-cell-specific essential functions are presented in Supplementary Methods 3. Overall, the validation confirmed that our constraint-based metabolic models specific to naïve CD4⁺ T cells, Th1, Th2, and Th17 cells represent relevant and realistic systems to examine drug response and predict drug targets.

Mapping existing and identifying potential drug targets in CD4⁺ T cells

We used the validated CD4⁺ T-cell-specific models to predict potential drug targets and combined it with the publicly available drug repurposing and tool compound data set from the Connectivity Map (cMap) database and mapped the approved drugs, clinical drug candidates, and tool compounds in the dataset with the metabolic genes in the models (Fig. 5a). Next, we performed in silico knock-outs of the associated drug target genes. Due to the presence of isozymes, not all the deleted target genes influenced the reaction(s). We identified 86, 79, 86, and 90 target genes whose deletion blocks at least one associated reaction in naïve, Th1, Th2, and Th17 models, respectively (Fig. 5b). In turn, these disruptions block multiple downstream reactions. Of these, 62 were common among four CD4⁺ T-cell subtypes (Fig. 5c). Four genes were targeted only in Th1 cells. All modeled gene deletions resulted in altered flux distributions that were quantified using flux ratios. For each drug target deletion, we classified all reactions into three categories (see Materials and methods): (1) reactions with decreased fluxes (down-reactions), (2) reactions with increased fluxes (up-reactions), and (3) reactions without any changes. We used these flux ratios to identify potential drug targets specific for immune diseases by exploring how disease-specific metabolic functions are affected upon each drug target inhibition.

First, we identified disease-specific metabolic functions for RA, MS, and PBC using differential gene expression analysis of publicly

Table 1. Model validation using specific behaviors.

Observation from literature	In silico experiment	Naïve	Th1	Th2	Th17	CD4 ⁺ T1670 (Naive)
1. Glucose transporter deficiency will inhibit the proliferation of cells ^{37,38}	Inhibited glucose transporters/remove glucose from the environment	↓growth ⁺	↓growth ⁺	↓growth ⁺	↓growth ⁺	No change [§]
2. CD4 ⁺ T cells produce lactate ³⁹	Observed if models have produced lactate	Lactate ⁺	Lactate ⁺	Lactate ⁺	Lactate ⁺	Lactate ⁺
3. Activated CD4 ⁺ T cells control pyruvate dehydrogenase function which in turn redirect pyruvate from entering the TCA cycle towards lactate production ³⁸	Increasing flux through pyruvate dehydrogenase reaction (PDHm) should decrease the lactate production	↓Lactate ⁺	↓Lactate ⁺	↓Lactate ⁺	↓Lactate ⁺	NA
4. During T-cell activation GAPDH is important for glycolysis ³⁸	Investigating if inhibition of GAPDH is impacting the growth	↓growth ⁺	0 growth ⁺	0 growth ⁺	0 growth ⁺	↓growth ⁺
5. Lack of transporters for Leucine impairs the metabolic reprogramming required for Th1 and Th17 ³⁸	Remove leucine from media and investigate the impact on growth	0 growth ⁺	0 growth ⁺	0 growth ⁺	0 growth ⁺	0growth ⁺
6. In T cells arginine deprivation leads to cell cycle arrest ³⁸	Remove arginine from the media and investigate the impact on growth	0 growth ⁺	0 growth ⁺	0 growth ⁺	0 growth ⁺	0growth ⁺
7. Gene acetyl-CoA carboxylase alpha (ACCC1) is essential for T-cell homeostasis ³⁸	Inhibit gene ACC1 or reaction Acetyl Coenzyme A Carboxylase (ACCOAC) and investigate the impact on growth	No change ^{§§}	0 growth ⁺	0 growth ⁺	0 growth ⁺	No change ^{§§}
8. Glutamine deficiency in media leads to low growth and proliferation ³⁸	Removing glutamine from media	↓growth ⁺	No change ^{§§}	No change ^{§§}	No change ^{§§}	No change ^{§§}

↓ = decrease, + = produced; † = agreement with literature; ‡ = partial agreement; § = disagreement; NA = experiment was not executed because infeasible.

(PES; see Materials and methods) for each drug target gene in each pair model/disease. PES represents the effect of gene inhibition on both upregulated and downregulated genes. A positive PES value for the drug target gene means that its inhibition decreases more fluxes controlled by genes upregulated in disease than it increases, or increases more fluxes controlled by genes downregulated in disease than it decreases. As such, inhibition of that gene target reverses the fluxes controlled by disease DEGs. In contrast, a negative PES means that the inhibition of a target gene increases more fluxes controlled by upregulated genes or decrease the more fluxes controlled by downregulated genes than the opposite. Among the different combinations of cell types and diseases, the PESs range was from -2 to 2 (Supplementary Fig. 14). Based on these considerations, genes with higher positive PES can serve as potential drug targets for the disease.

Using PES as a measure of target relevance, we identified 62 potential drug targets that were common to our models (Fig. 5c). These genes displayed various PES ranks across models and diseases. To choose drug targets that performed better across different CD4⁺ T cells, we considered PES ranks of the four subtype-specific models. First, we normalized the PES ranks by transforming them into Z-scores in each model. Since the studied autoimmune diseases typically involve more than one type of CD4⁺ T-cell subtype, we next summed up the Z-scores of all the models within a disease for each drug target (Supplementary Fig. 14). A minimum aggregate Z-score represents overall high PES ranks predicted across four cell types. Therefore, a gene with a minimum aggregated Z-score could be a potential high confidence drug target. We used a Z-score cutoff of -1 (1 standard deviation lower than the mean aggregated Z-score) and identified 17, 27, and 24 potential drug targets for RA, MS, and PBC, respectively (Table 2; see more details in Supplementary Table 2). Ranking based on aggregated Z-scores is provided in Supplementary Data 9. Taken together, our combined use of the disease-matched genome-scale metabolic models of CD4⁺ T cells and the well target-annotated public dataset of bioactive compounds generated a manageable list of potential drug targets suitable for deeper analysis and follow-up.

Analysis and validation of predicted drug targets

To further analyze and validate our target list, we performed a comprehensive literature survey (Table 2; see more details in Supplementary Table 2). Among the 17 suggested drug targets for RA, dihydroorotate dehydrogenase (DHODH) and Acetyl-CoA acetyltransferase (ACAT1) have already been explored as targets in drug development efforts^{42,43}, and 15 genes were newly identified. Among these, eight (LSS, NAMPT, FDPS, SQLE, EPHX2, CAT, CS, SOD2) have been found to inhibit CD4⁺ T-cell proliferation upon deletion (Table 2; see more details in Supplementary Table 2). The product of the reaction catalyzed by 4-Aminobutyrate Aminotransferase (ABAT) is linked to RA. Dysregulation of other genes, such as pyruvate dehydrogenase E1 (PDHB), Farnesyl-diphosphate farnesyltransferase 1 (FDF1), Oxoglutarate Dehydrogenase (OGDH), alpha-galactosidase (GAA), has not been previously reported to impact CD4⁺ T-cell proliferation.

Furthermore, we predicted 27 possible drug targets for MS. Of these, glutathione reductase (GSR) and dihydrofolate reductase (DHFR) were already explored as targets using the experimental autoimmune encephalomyelitis (EAE) model^{44,45} and 25 genes were newly identified. Among these, 12 (CAT, IDH2, HMGCR, PKM, ABAT, LSS, FASN, PPAT, PNP, CS, CAD, SQLE) have been previously reported inhibiting CD4⁺ T-cell proliferation upon deletion. Genes that were not previously reported to affect CD4⁺ T cells upon deletion include Carnitine O-palmitoyltransferase 2 (CPT2), MP cyclohydrolase (ATIC), Ornithine decarboxylase (ODC1),

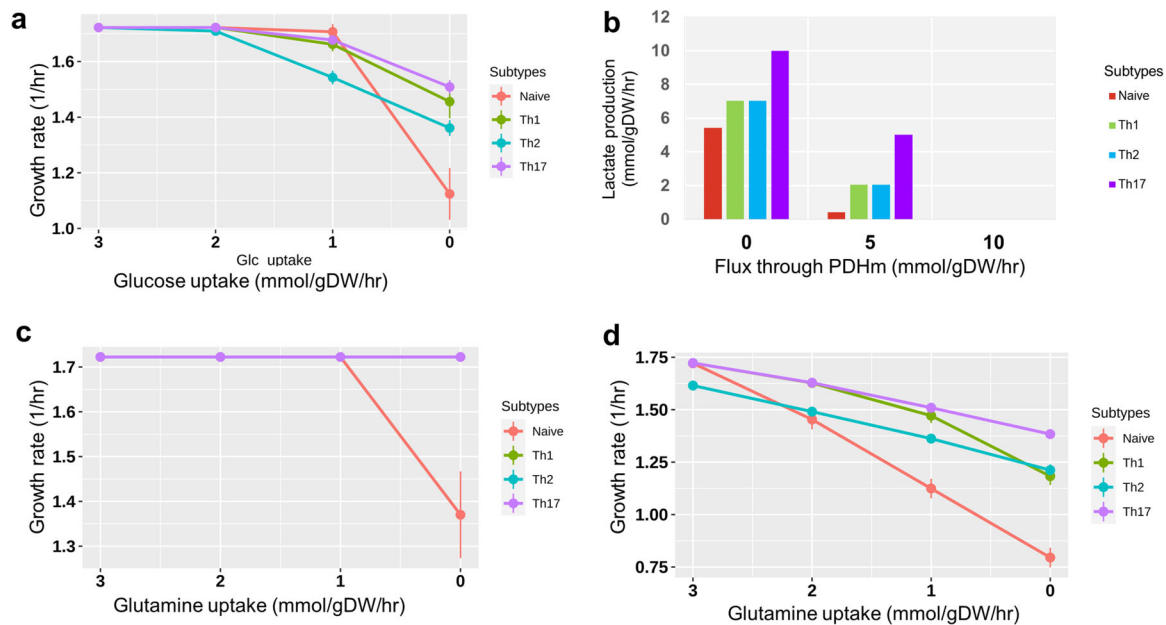


Fig. 4 Model predictions are consistent with the literature. a Dependency of growth rate (in all models) on glucose uptake when glucose was available (>5 mmol/g DW/hr). **b** Production of lactate with increased flux through pyruvate dehydrogenase. **c** The dependency of growth rate (in all models) on glutamine when glucose was available (>5 mmol/g DW/hr). **d** The dependency of growth on glutamine when glucose was removed from the environment. Dots in **a**, **c**, and **d** are average flux and error bars are standard deviation ($n = 5$). We varied the uptake rate of glucose or glutamine five times ($n = 5$) to obtain the average and standard deviation at each dot. For example, in **a**, the growth rate at 3.0 mmol/g DW/hr glucose uptake is the average of growth rates obtained under 3.2, 3.1, 3.0, 2.9, 2.8 (mmol/g DW/hr) of glucose uptake.

Dihydropyrimidine dehydrogenase (DPYD), and Farnesyl-diphosphate farnesyltransferase (FDFT1).

Finally, we identified 24 possible drug targets for PBC. None of them was previously explored as a drug target in PBC. The deletion of seven of these potential gene targets (NAMPT, EPHX2, FASN, ADA, SLC2A3, TXNRD1, ACLY) has been reported to affect $CD4^+$ T cells in the literature. Genes that have not yet been reported to affect $CD4^+$ T cells upon deletion include Long-chain-fatty-acid-CoA ligase 3 (ACSL3), Adenosine kinase (ADK), and S-adenosylmethionine decarboxylase proenzyme (AMD1).

43 of the 68 predicted drug targets were found for only one disease. Six drug targets (LSS, ABAT, SQLE, FDFT1, CAT, CS) were common to RA and MS; five drug targets (NAMPT, EPHX2, COMT, HIBCH, GAA) were common to RA and PBC; and two drug targets (ADH5, FASN) were common to MS and PBC. We show the drugs and compounds available for these targets in Table 3. Out of the 55 unique drug targets identified across three diseases, 38 were robust across different cutoffs (Supplementary Methods 9). A few examples of drug targets from purine metabolism, fatty acid synthesis, and the TCA cycle are shown in Fig. 6.

Experimental validation

Next, we experimentally validated our predictions by targeting genes that have not been reported in the literature to suppress $CD4^+$ T-cell proliferation. We selected ten FDA-approved drugs based on their association with reactions belonging to pathways we were interested in, while ensuring they would cover at least one target from each disease. Four of the tested drugs indeed resulted in decreased $CD4^+$ T-cell proliferation. Genes targeted by these drugs include COMT (RA, PBC), CPT2 (MS), DPYD (MS), and ACSL3 (PBC). COMT is associated with five different reactions of the tyrosine metabolism (Fig. 6f). The genes CPT2 and ACSL3 both catalyze the production of long-chain Acyl-CoA in fatty acid biosynthesis from different substrates (Fig. 6c). DPYD catalyzes the production of uracil and thymine from dihydrouracil and dihydrothymine in pyrimidine metabolism. We subjected human $CD4^+$ T cells stimulated with TCR signaling and IL-2 to different

doses of drugs for 48 h and 72 h. Their proliferation was assessed by the MTT colorimetric cell proliferation assay (Fig. 7). A reduction of $CD4^+$ T-cell proliferation was observed for every chosen drug. Entacapone, targeting the COMT gene, showed significant activity at 48 h and 72 h at 100 μ M and 1000 μ M (Fig. 7a). EPA, targeting ACSL3, decreased proliferation at the highest dose (1000 μ M) at 72 h, while the other concentrations did not significantly affect proliferation (Fig. 7b). Perhexiline, targeting CPT2, also reduced proliferation at 72 h at 100 μ M and 1000 μ M (Fig. 7c). Fluorouracil, targeting DPYD, is the only drug that showed an effective impact on $CD4^+$ T-cell proliferation at a lower dose (1 μ M) at 72 h (Fig. 7d). Interestingly, Entacapone, Perhexiline exhibit a significant enhancement of proliferation at a low dose (1 μ M), indicating that these drugs can present a biphasic effect in T-cell proliferation. Our experimental validations thus indicate that the perturbation of the activity of our predicted targets can impact $CD4^+$ T-cell proliferation in a time and dose-dependent manner, as we have recently envisioned⁴⁶.

Six drugs showed no or opposite effect on the T-cell proliferation, including DFMO, Pemetrexed, N6022, Ethyl-pyruvate, Pyrazinamide, and Quercetin. As an example, Fig. 7e shows that DFMO, targeting ODC1, does not impact T-cell proliferation with the indicating dose. The data for the other five drugs are shown in Supplementary Fig. 15.

Taken together, our analysis has identified 68 possible drug targets of relevance to metabolic regulation of autoimmune diseases. We discuss the implications of our results in more detail below.

DISCUSSION

Our predicted drug targets were classified into two categories: validated and potential. We considered a target to be validated if previously explored as such in the context of RA, MS, and/or PBC. Potential targets, those not previously reported as such for the three diseases we focused on here, were further classified into three subcategories: target genes that are supported by published

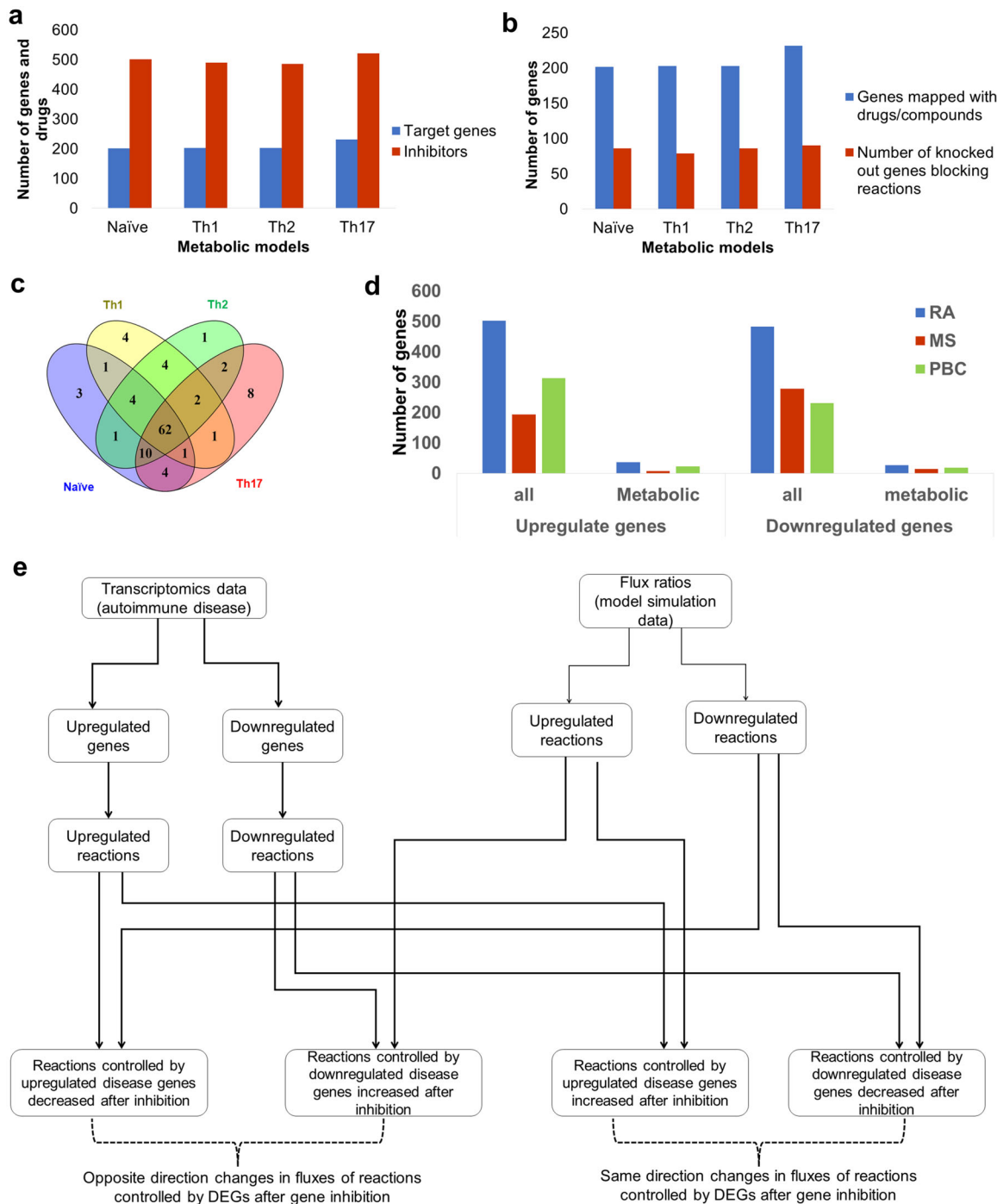


Fig. 5 Identification of potential drug targets for RA, MS, and PBC. **a** Distribution of metabolic drug target genes, and inhibitory drugs or compounds in each model. **b** Number of metabolic genes in the models mapped with inhibitory drugs (blue bars) and number of genes among drugs mapped genes that can block at least one reaction upon inhibition (red bars). **c** Comparison of metabolic drug targets that affect reactions upon deletion in CD4⁺ T-cell models. **d** Number of all differentially expressed genes (DEGs) and metabolic DEGs in three diseases rheumatoid arthritis (RA), multiple sclerosis (MS), and primary biliary cholangitis (PBC) ($P_{\text{adj}} < 0.05$). The DEGs were analyzed using three transcriptomics datasets (one dataset per disease). The data were obtained from peripheral CD4⁺ T cells of groups of patients and healthy individuals. **e** Schematic representation of the integration of disease-associated differentially expressed genes and affected reaction on each drug target gene perturbation. For each drug target deletion, we investigated how many of fluxes regulated by upregulated genes are decreased and fluxes regulated by downregulated genes are increased. We used these numbers to calculate PES (perturbation effect score, see Materials and methods).

experimental data, predicted target genes for which no data is currently available, and predicted drug targets for which we provide experimental validation. We will discuss select examples of targets in each of these categories to illustrate ways in which

our model and analysis can be used to advance future drug repurposing as well as drug discovery efforts.

Our predictions include three genes (*DHODH*, *ACAT1*, and *DHFR*) that code for proteins targeted by approved drugs currently used

Table 2. Identified CD4⁺ T-cell drug targets for autoimmune diseases.

Disease	Gene	Experimental evidence relevant to CD4 ⁺ T cells and autoimmune diseases
RA	Lanosterol synthase (LSS)	Inhibition of lanosterol synthase (LSS) might decrease the endogenous cholesterol that may lead to impact cell division ⁹⁷ .
	4-aminobutyrate aminotransferase (ABAT)	GABA downregulates inflammatory response in a mouse model of RA ⁴² ; inhibition of ABAT might increase GABA ¹⁶ .
	Nicotinamide phosphoribosyltransferase (NAMPT)	Nampt inhibition reduces demyelination and disability in EAE ⁵⁶), lack of NAMPT expression affect T-cell development ⁹⁸ .
	Farnesyl pyrophosphate synthase (FDPS)	Inhibition of FDPS inhibits T-cell cytokine production ⁹⁹ .
	Squalene monooxygenase (SQLE)	Increased membrane cholesterol in T cells leads to an inflammatory response ¹⁰⁰ .
	Farnesyl-diphosphate farnesyltransferase (FDFT1)	No support
	Bifunctional epoxide hydrolase 2 (EPHX2)	Inhibition of EPHX2 pre-clinically evaluated as a drug target for IBD ⁵⁸ .
	2-oxoglutarate dehydrogenase (OGDH)	No support
	Catalase (CAT)	Protect T cells against oxidative stress ¹⁰¹ .
	Citrate synthase (CS)	Inhibition of citrate synthase leads to a reduction in citrate, leading to reduced proliferation ¹⁰² .
	Pyruvate dehydrogenase E1 component subunit beta (PDHB)	No inhibition of CD4 ⁺ T-cell proliferation under treatment with drug ethyl-pyruvate (This study)
	Catechol O-methyltransferase (COMT)	Reduced CD4 ⁺ T-cell proliferation when inhibited using drug entacapone (This study)
	3-hydroxyisobutyryl-CoA hydrolase (HIBCH)	No inhibition of CD4 ⁺ T-cell proliferation under treatment with drug quercetin (This study)
	Superoxide dismutase [Mn], mitochondrial (SOD2)	Loss of SOD2 increased superoxide, and defective T-cell development ⁶² .
	Dihydroorotate dehydrogenase (DHODH)	Explored as a potential drug target for RA ⁴³ and MS ¹⁰³ .
	Alpha-glucosidase (GAA)	No support
	Acetyl-CoA acetyltransferase, mitochondrial (ACAT1)	Target of sulfasalazine that is anti-inflammatory indicated for the treatment of ulcerative colitis and rheumatoid arthritis ⁵⁰ .
MS	Carnitine O-palmitoyltransferase 2 (CPT2)	Reduced CD4 ⁺ T-cell proliferation when inhibited using drug perhexiline (This study)
	Catalase (CAT)	Protect T cells against oxidative stress ¹⁰¹ .
	ATP synthase subunit alpha (ATP5F1A)	No inhibition of CD4 ⁺ T-cell proliferation under treatment with drug quercetin (This study)
	ATP synthase subunit beta (ATP5F1B)	No inhibition of CD4 ⁺ T-cell proliferation under treatment with drug quercetin (This study)
	ATP synthase F1 subunit gamma (ATP5F1C)	No inhibition of CD4 ⁺ T-cell proliferation under treatment with drug quercetin (This study)
	Ornithine decarboxylase (ODC1)	No inhibition of CD4 ⁺ T-cell proliferation under treatment with drug DFMO (This study)
	MP cyclohydrolase (ATIC)	No inhibition of CD4 ⁺ T-cell proliferation under treatment with drug pemetrexed(This study)
	ATP synthase subunit delta (ATP5F1D)	No support
	ATP synthase F(0) complex subunit B1 (ATP5PB)	No support
	Alcohol dehydrogenase class-3 (ADH5)	No inhibition of CD4 ⁺ T-cell proliferation under treatment with compound N6022 (This study)
	Dihydropyrimidine dehydrogenase (DPYD)	Reduced CD4 ⁺ T-cell proliferation when inhibited using drug perhexiline (This study)
	Isocitrate dehydrogenase (IDH2)	Knockdown of IDH1 or IDH2 reduces IL-17 producing cells (Patent WO2017123808A1) ¹⁰⁴ .
	Glutathione reductase (GSR)	Inhibition of GSH de novo synthesis reduces the pathological progression of EAE ⁴⁴ .
	3-hydroxy-3-methylglutaryl-coenzyme A reductase (HMGCR)	Potential target for autoimmune diseases ¹⁰⁵ .
	Farnesyl-diphosphate farnesyltransferase (FDFT1)	No support
	Dihydrofolate reductase (DHFR)	Low dose methotrexate (inhibitor of DHFR) found effective for MS, RA, and Crohn's disease ⁴⁵ .
	Pyruvate kinase (PKM)	Potential target to regulate inflammation ⁵⁹ .
	Phosphoribosylglycinamide formyltransferase (GART)	No inhibition of CD4 ⁺ T-cell proliferation under treatment with drug pemetrexed (This study)
	4-aminobutyrate aminotransferase (ABAT)	GABA downregulates inflammatory response in a mouse model of RA ⁴² ; inhibition of ABAT might increase GABA ¹⁶ .

Table 2 continued

Disease	Gene	Experimental evidence relevant to CD4 ⁺ T cells and autoimmune diseases
	Lanosterol synthase (LSS)	Inhibition of lanosterol synthase (LSS) might decrease the endogenous cholesterol, leading to impact cell division ⁹⁷ .
	Fatty acid synthase (FASN)	Fatty acid synthase linked to the pathogenicity of Th17 cells ¹⁰⁶ .
	Phosphoribosyl pyrophosphate amidotransferase (PPAT)	Knockdown of CAD and PPAT promotes regulatory CD4 ⁺ T cells ¹⁰⁷ .
	Purine nucleoside phosphorylase (PNP)	inhibition leads to T-cell suppression ¹⁰⁸ .
	Citrate synthase (CS)	Increased citrate in MS patients ¹⁰⁹ .
	ADP/ATP translocase 3 (SLC25A6)	No support
	Carbamoyl-phosphate synthetase 2 (CAD)	Knockdown of CAD and PPAT promotes regulatory CD4 ⁺ T cells ¹⁰⁷ .
	Squalene monooxygenase (SQLE)	Increased membrane cholesterol in T cells leads to an inflammatory response ¹⁰⁰ .
PBC	Nicotinamide phosphoribosyltransferase (NAMPT)	Nampt inhibition reduces demyelination and disability in EAE ⁵⁶ , lack of NAMPT expression affect T-cell development ⁹⁸ .
	Inosine triphosphate pyrophosphatase (ITPA)	No support
	Adenosine kinase (ADK)	No support
	Long-chain-fatty-acid-CoA ligase 3 (ACSL3)	Reduced CD4 ⁺ T-cell proliferation when inhibited using drug EPA (This study)
	Thymidine phosphorylase (TYMP)	No support
	S-adenosylmethionine decarboxylase proenzyme (AMD1)	No support
	Adenine phosphoribosyltransferase (APRT)	No support
	Alcohol dehydrogenase class-3 (ADH5)	No support
	Catechol O-methyltransferase (COMT)	Reduced CD4 ⁺ T-cell proliferation when inhibited using drug entacapone (This study)
	Bifunctional epoxide hydrolase 2 (EPHX2)	Inhibition of EPHX2 pre-clinically evaluated as drug target for IBD ⁵⁸ .
	3-hydroxyisobutyryl-CoA hydrolase (HIBCH)	No inhibition of CD4 ⁺ T-cell proliferation under treatment with drug quercetin (This study)
	Fatty acid synthase (FASN)	Fatty acid synthase linked to the pathogenicity of Th17 cells ¹⁰⁶ .
	Beta-galactosidase (GLB1)	No support
	Phosphatidylglycerophosphatase and protein-tyrosine phosphatase 1 (PTPMT1)	No support
	Adenosine deaminase (ADA)	ADA is a potential target for the treatment of inflammatory disorders ¹¹⁰ .
	Lactoylglutathione lyase (GLO1)	No support
	Glucose-6-phosphate 1-dehydrogenase (G6PD)	No support
	Hypoxanthine-guanine phosphoribosyltransferase (HPRT1)	No support
	Alpha-glucosidase (GAA)	No support
	Solute carrier family 2, facilitated glucose transporter member 3 (SLC2A3)	Glut3 expressed in differentiated cells and resting equals to glut1 ³⁷ .
	Multidrug resistance-associated protein 1 (ABCC1)	No support
	Thioredoxin reductase 1 (TXNRD1)	Essential for DNA synthesis during T-cell metabolic reprogramming and proliferation ¹¹¹ .
	Superoxide dismutase (SOD1)	No support
	ATP-citrate synthase (ACLY)	Inactivation of ACLY reduces IL-2-promoted CD4 ⁺ T-cell growth ¹¹² .

to treat autoimmune diseases^{42–45,47}. A strong example of an already validated drug target predicted by our models is dihydroorotate dehydrogenase (DHODH), a key enzyme in the de novo pyrimidine synthesis pathway, and a target of leflunomide, an approved drug for rheumatoid arthritis^{43,48}. DHFR (dihydrofolate reductase) is a well-established oncology drug target, and also an immunosuppressant and anti-inflammatory target⁴⁹. Low doses of an FDA-approved DHFR inhibitor methotrexate have been found effective as a treatment for MS, RA, and Crohn's disease⁴⁵. Mitochondrial acetyl-CoA acetyltransferase (ACAT1) is a target for FDA approved anti-inflammatory drug sulfasalazine in inflammatory bowel syndrome. Furthermore, this drug is indicated for treatment for rheumatoid arthritis and ulcerative colitis⁵⁰. Taken together, our models successfully

replicated current clinical practice, further strengthening the value of our approach.

Interestingly, a major subcategory of gene targets we identified code for proteins that have not previously been explored for the treatment of RA, MS, and PBC. We can now use these insights to formulate preclinical and clinical hypotheses. For example, *ABAT*, which encodes the GABA-transaminase enzyme that breaks down γ -aminobutyric acid (GABA; a neurotransmitter), was identified in our analysis as a potential target. While *ABAT* has not been previously identified as a drug target for RA, we can hypothesize that its inhibition may increase free GABA levels which would, in turn, inhibit CD4⁺ T-cell activation. The relationship between GABA levels and suppressions of CD4⁺ T-cell activation has been previously reported, further suggesting a link between neurotransmission and immune response^{51–53}. There are currently two

Table 3. Drugs and compounds for identified drug targets.

Gene description	Drugs/compound ^a	Status of drugs/compounds ^a
Lanosterol synthase (LSS)	RO-48-8071	Preclinical
4-aminobutyrate aminotransferase (ABAT)	Vigabatrin, phenelzine, valproic acid	launched
Nicotinamide phosphoribosyltransferase (NAMPT)	FK866	Phase 2
Farnesyl pyrophosphate synthase (FDPS)	Pamidronic acid, Zoledronic acid, Alendronic acid, Ibandronate, Risedronic acid	Launched
Squalene monooxygenase (SQLE)	Ellagic-acid	Phase 2
Farnesyl-diphosphate farnesyltransferase (FDFT1)	TAK-475	Investigational
Bifunctional epoxide hydrolase 2 (EPHX2)	GSK2256294A	Phase 1
2-oxoglutarate dehydrogenase (OGDH)	Valproic acid	Launched
Catalase (CAT)	Fomepizole	Launched
Citrate synthase (CS)	Oxaloacetate	Phase 2/phase 3
Pyruvate dehydrogenase E1 component subunit beta (PDHB)	2-oxopropanoate	Preclinical
Catechol O-methyltransferase (COMT)	Entacapone, Nitecapone, Opicapone	Launched, Phase 2, phase 3
3-hydroxyisobutyryl-CoA hydrolase (HIBCH)	Quercetin	Launched
Superoxide dismutase [Mn], mitochondrial (SOD2)	Tetraethylenepentamine	Phase 2/ Phase 3
Dihydroorotate dehydrogenase (DHODH)	Atovaquone, Leflunomide, Teriflunomide, Brequinar	Launched
Alpha-glucosidase (GAA)	Miglitol, Acarbose	Launched
Acetyl-CoA acetyltransferase, mitochondrial (ACAT1)	Sulfasalazine	Launched
Carnitine O-palmitoyltransferase 2 (CPT2)	Perhexiline	Launched
ATP synthase subunit alpha (ATP5F1A)	Quercetin	Launched,
ATP synthase subunit beta (ATP5F1B)	Quercetin	Launched
ATP synthase F1 subunit gamma (ATP5F1C)	Quercetin	Launched
Ornithine decarboxylase (ODC1)	MC-1, Putrescine, DFMO	Phase 3, Phase 2, launched
MP cyclohydrolase (ATIC)	Pemetrexed	Launched
ATP synthase subunit delta (ATP5F1D)	Sevoflurane, Enflurane, Methoxyflurane	Launched
ATP synthase F(0) complex subunit B1 (ATP5PB)	BTB06584	Preclinical
Alcohol dehydrogenase class-3 (ADH5)	N6022	Phase 1/Phase 2
Dihydropyrimidine dehydrogenase (DPYD)	5-fluorouracil, Gimeraci	Launched
Isocitrate dehydrogenase (IDH2)	AGI-6780	Preclinical
Glutathione reductase (GSR)	Carmustine	Launched
3-hydroxy-3-methylglutaryl-coenzyme A reductase (HMGCR)	Atorvastatin, Fluvastatin, Lovastatin, Meglitol, Pitavastatin, Pravastatin, Rosuvastatin, Simvastatin, Nadide	Launched
Dihydrofolate reductase (DHFR)	Aminopterin, Chlorproguanil, Methotrexate, Pralatrexate, Proguanil, Pyrimethamine, Sulfameter, Trimethoprim, Pemetrexed	Launched
Pyruvate kinase (PKM)	TEPP-46, 2-oxopropanoate	Preclinical
Phosphoribosylglycinamide formyltransferase (GART)	Pemetrexed	Launched
Fatty acid synthase (FASN)	Pyrazinamide, Cerulenin	Launched
Phosphoribosyl pyrophosphate amidotransferase (PPAT)	Azathioprine, Mercaptopurine	Launched
Purine nucleoside phosphorylase (PNP)	Acyclovir, Didanosine	Launched
ADP/ATP translocase 3 (SLC25A6)	Clodronic-acid	Launched
Carbamoyl-phosphate synthetase 2 (CAD)	Sparfosate	Phase 3
Inosine triphosphate pyrophosphatase (ITPA)	Citric-acid	Preclinical
Adenosine kinase (ADK)	ABT-702	Preclinical
Long-chain-fatty-acid-CoA ligase 3 (ACSL3)	Eicosapentaenoic acid	Launched
Thymidine phosphorylase (TYMP)	Tipiracil	Launched
S-adenosylmethionine decarboxylase proenzyme (AMD1)	Ademetionine, Putrescine	Launched, Phase 2
Adenine phosphoribosyltransferase (APRT)	Citric acid	Preclinical
Beta-galactosidase (GLB1)	Fagomine	Phase 2
Phosphatidylglycerophosphatase and protein-tyrosine phosphatase 1 (PTPMT1)	Alexidine	Preclinical

Table 3 continued

Gene description	Drugs/compound ^a	Status of drugs/compounds ^a
Adenosine deaminase (ADA)	Cladribine, Pentostatin, Dipyridamole, Fludarabine	Launched
Lactoylglutathione lyase (GLO1)	Indomethacin	Launched
Glucose-6-phosphate 1-dehydrogenase (G6PD)	RRx-001	Phase 2
Hypoxanthine-guanine phosphoribosyltransferase (HPRT1)	Azathioprine, Mercaptopurine	Launched
Solute carrier family 2, facilitated glucose transporter member 3 (SLC2A3)	2-deoxyglucose	Phase 2
Multidrug resistance-associated protein 1 (ABCC1)	Reversan, Ko143	Preclinical
Thioredoxin reductase 1 (TXNRD1)	Fotemustine	Launched
Superoxide dismutase (SOD1)	Tetraethylenepentamine	Phase 2/Phase 3
ATP-citrate synthase (ACLY)	ETC-1002	Phase 3

^aData obtained from repurposing tool⁸⁴ of cMap database and DrugBank⁵⁰.

FDA-approved drugs, vigabatrin, and phenelzine, that target ABAT. Although we do not expect that either one of these agents can be repurposed to treat autoimmune disease given that they are an anti-seizure medicine and an antidepressant, respectively, we propose that further analysis of relationships between neurotransmission and immune response offers an interesting targeting opportunity⁴². Another example is glutathione reductase (GSR), an enzyme that reduces oxidized glutathione disulfide to cellular antioxidant GSH⁵⁴. It has been shown that inhibition of the de novo GSH synthesis can reduce the pathological progression of experimental autoimmune encephalomyelitis (EAE)⁴⁴. Here, carmustine, a chemotherapy drug, is an FDA-approved drug that targets GSR, offering a viable starting point for future pre-clinical testing (Table 3). Additional high confidence predictions and target candidates are a group of genes that have been experimentally shown to repress CD4⁺ T cells upon inhibition. This list includes nicotinamide phosphoribosyltransferase (NAMPT), which we now predict is a drug target for RA. This enzyme is involved in NAD⁺ synthesis⁵⁵ and was previously explored as a drug target in EAE for MS⁵⁶, melanoma, T-cell lymphoma, and leukemia⁵⁷. Given that two NAMPT inhibitors, GMX1778 and FK-866, are in phase II clinical trials (Table 3), this enzyme represents a target where pre-clinical testing and follow-up may lead to drug repurposing opportunities. Another example worth highlighting is epoxide hydrolase 2 (EPHX2), which converts toxic epoxides to non-toxic dihydrodiols^{54,55}. Its inhibition was reported to decrease the production of proinflammatory cytokines in preclinical evaluation in inflammatory bowel syndrome⁵⁸. For EPHX2, an inhibitor GSK2256294A is in phase I clinical trial, indicating that developing drugs for this target may be possible. Moreover, our model implicated enzymes such as pyruvate kinase (PKM), which impacts glycolysis, HMG-CoA reductase (HMGCR), which regulates cholesterol biosynthesis, and adenosine deaminase (ADA), which converts harmful deoxyadenosine to not harmful deoxyinosine. Each of these enzymes has been experimentally linked to T-cell proliferation and development^{59–61}, and all three targets have been the subject of previous drug development campaigns (Table 3). ATP Citrate Lyase (ACLY), Catalase (CAT), Farnesyl diphosphate synthase (FDPS), Lanosterol synthase (LSS), Squalene epoxidase (SQLE), and Superoxide dismutase 2 (SOD2) also represent targets we identified. SQLE is involved in cholesterol biosynthesis, and in general agreement with recent reports that inhibiting cholesterol pathways can suppress T-cell proliferation⁶⁰. The loss of SOD2 can increase superoxides and defective T-cell development⁶². For all these targets, either preclinical, clinical, or approved inhibitors are available, which we consider encouraging for further study and drug repurposing (see Table 3 for details).

Other predicted genes are part of the TCA cycle (Citrate synthase (CS), Isocitrate dehydrogenase 2 (IDH2)), ribonucleotide biosynthetic processes (Phosphoribosyl pyrophosphate amidotransferase (PPAT), Carbamoyl-phosphate synthetase 2, Aspartate transcarbamylase, and Dihydroorotase (CAD)), and lipid biosynthesis (Fatty acid synthase (FASN)) that are also important for T cell development. As with the examples above, many of these potential candidate targets have inhibitors that are in different stages of preclinical and clinical development, and some (like PPAT and FASN inhibitors) have been FDA approved (Table 3).

In addition to gene targets with robust or partial existing experimental evidence, we identified 31 potential gene targets for which no evidence currently exists. These genes are involved in glycolysis, TCA cycle, OXPHOS, and the metabolism of fatty acid, pyruvate, purine, pyrimidine, arginine, proline, and tyrosine, which are all critical for T-cell activation and proliferation^{39,63}. We performed in vitro experiments to investigate predicted targets without existing published evidence and we tested ten FDA-approved drugs. In four cases of drug targets (COMT, ACSL3, CPT2, and DPYD), the drugs (entacapone, EPA, perhexiline, and fluorouracil, respectively) inhibited the proliferation of CD4⁺ T cells in a dose and time-dependent manner. Some drugs displayed a “biphasic effect” where it encouraged proliferation at a low dose while inhibiting T-cell proliferation at a higher dose. This dose–response effect, called hormesis, is usually an adaptive survival response to toxic agents or stressful environments. Hormetic effects are, in general, produced by highly conserved evolutionary systems and characterized by the coordinated activation of molecular signals triggering coherent metabolic responses to maintain cell homeostasis⁶⁴. Indeed, it is well established that the ability of T cells to modulate their metabolism upon environmental changes is key to preserve their survival and fulfill their functions⁶⁵. In the case of ODC1, we did not observe any impact on CD4⁺ T-cell proliferation under any tested concentration of DFMO at both 48 and 72 h. It is difficult to explain this lack of effect without further experimental investigations. It might be that ODC1 is in large excess in our cell cultures, or that the amount of active enzyme is tightly regulated.

Collectively, our models and approach led to the identification of potential high-value targets for RA, MS, and PBC treatment, and proposed several drugs in current clinical use for drug repurposing.

Data integration enabled us to build, refine, and validate high-quality cell-type-specific models. While many of the major pathways important for CD4⁺ T-cell activation and proliferation are commonly active across different CD4⁺ T-cell subtypes we tested, the models differ with respect to how these pathways are used for growth. For example, higher activity of the fatty acid

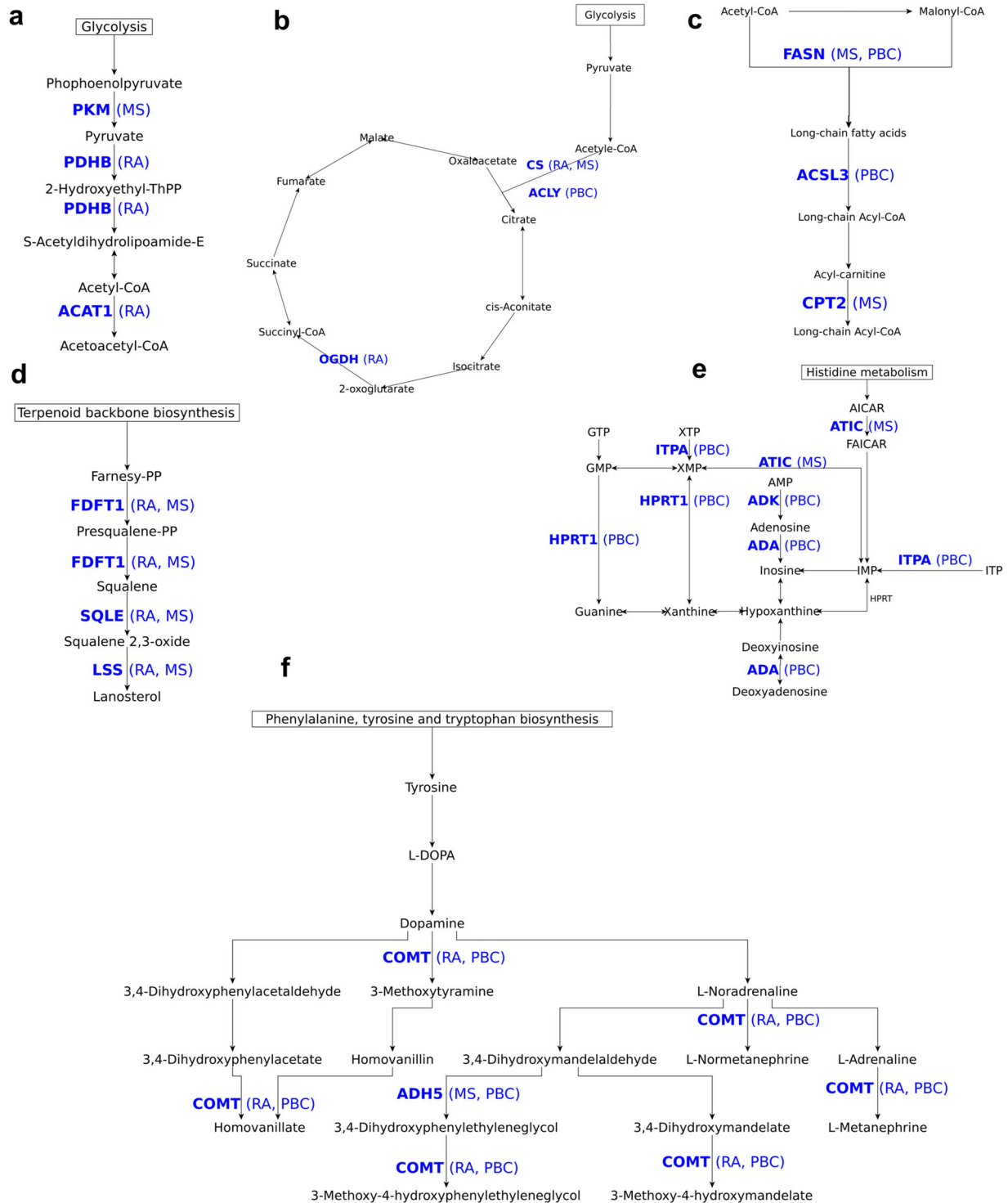


Fig. 6 Examples of identified drug targets mapped on the metabolic pathways. Relevant sub-networks of pathways where drug targets were mapped are shown for **a** pyruvate metabolism, **b** TCA cycle, **c** fatty acid biosynthesis, **d** steroid biosynthesis, **e** purine metabolism, and **f** tyrosine metabolism. The mapped drug targets (bold font) and diseases (in brackets) are shown in blue colored text.

oxidation pathway is more important in naïve but not in effector CD4⁺ T cells that have elevated glycolysis⁶³ and fatty acid synthesis pathways. A substantial number of essential genes identified from these models overlapped with gene essentiality data obtained from different cell lines⁴¹. When compared to gene essentiality from independent cell line data, the effector cell models performed slightly better than the naïve model. One possible reason for this difference might be the difference in

nutrient preferences between naïve and effector T cells. We are conscious that assessing model performances based on comparison with essential genes defined on different cell lines is not ideal. Properly assessing their accuracy would require CD4⁺ T-cell-specific essentiality data. Integration of disease-associated DEGs with flux profiles under gene knock-out helped us to select disease-specific drug targets. While computational models of signal transduction in CD4⁺ T cells^{66,67} are available, metabolic

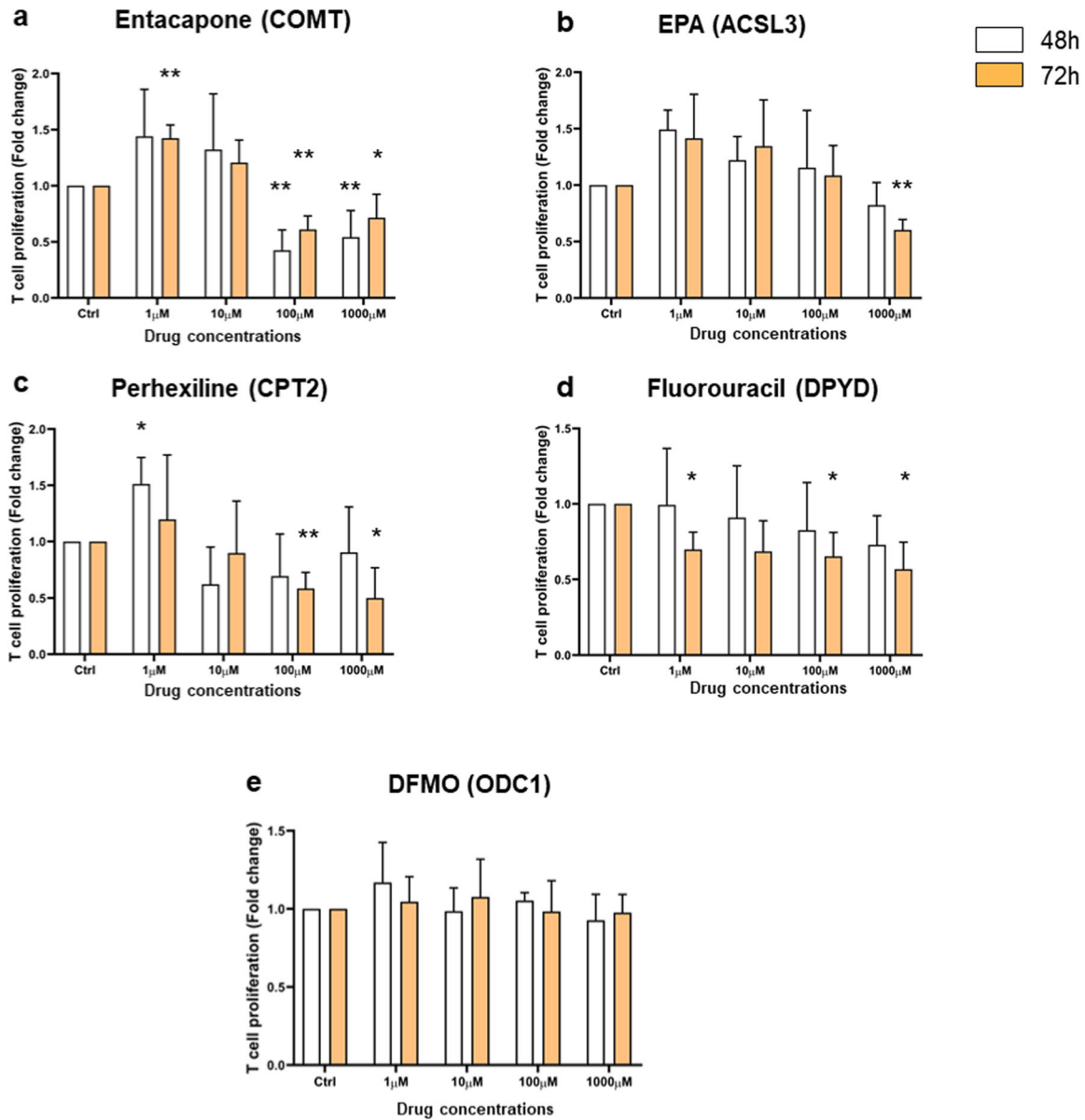


Fig. 7 Analysis of CD4⁺ T-cell proliferation response upon drug treatment by MTT assay. CD4⁺ T cells were exposed to various concentrations of drugs (1, 10, 100, and 1000 μ M) for 48 h (white bars) and 72 h (orange bars). Drugs' names (Entacapone, EPA, Perhexiline, Fluorouracil, and DFMO) were indicated on the top of each graph bar with their corresponding targeted gene in parentheses. Cell proliferation is expressed as fold change \pm SEM relative to untreated control cells and is representative of four independent experiments. Statistic significance was only shown for effective concentration and was evaluated using a paired *t*-test, one-tailed (* p < 0.05, ** p < 0.005).

models of effector and regulatory CD4⁺ T cells have not been developed (except for naïve CD4⁺ T cells³⁴). Similar metabolic models were previously used to predict drug targets against pathogens¹⁸ and complex diseases such as cancers⁶⁸.

While our approach can be generalized for human diseases and used with any -omics dataset, the unavailability of reliable data contributes to some limitations. Because of heterogeneity with respect to time after stimulation with cytokines in the available datasets, constructed models represent inclusive metabolic phenotypes during activation and proliferation for each CD4⁺ T-cell subtype. Thus, time-specific data would be required to study metabolic phenotype at a specific time point in CD4⁺ T-cell development. Furthermore, by integrating gene expression and proteomics data, we improved the identification of expressed genes compared with the sole use of gene expression or proteomics datasets. This approach presents certain limitations

because of post-transcriptional and post-translational modifications. Integrating more functional data such as enzyme activities and measured metabolic fluxes could further improve the selection of active reactions within the context of specific models. In addition, the biomass objective function used in our study is not specific to CD4⁺ T cells. We used a biomass objective function generated for human alveolar macrophages. Differences in growth conditions and the respective sizes of macrophages and CD4⁺ T cells might impact the ratios of precursors used for biomass objective functions. Since the precursors for biomass production would be the same across different cell types, in the absence of comprehensive data on precursor ratios from a specific cell type, the objective function of similar cells is useful for obtaining flux distribution. A specific objective function that considers varying utilization of precursor metabolites (such as glycolysis intermediates) by different CD4⁺ T cells for biomass production might

further improve the models. However, we have shown that changing objective functions (from the Recon3D to macrophage model) had no significant impact on the constructed models (see Materials and methods for details). Similarly, reliable disease-specific data were unavailable for specific CD4⁺ T-cell subtypes, therefore, building subtype-specific cell metabolic models under disease conditions was not possible. We mitigated this limitation by integrating disease-specific DEGs from sorted CD4⁺ T cells with models, which resulted in metabolic fluxes relevant to diseases. In the future, with the availability of more disease and cell-type-specific data, our integrative approach may further improve these results. In particular, we hope to include other cell-types such as T follicular helper (Tfh), T helper 9 (Th9), and T helper 22 (Th22) cells, which also play a role in the development of autoimmune diseases.

Overall, our integrative systems modeling approach has provided a new perspective for the treatment of RA, MS, and PBC. Moreover, the newly constructed models may serve as tools to explore the metabolism of CD4⁺ T cells. Additionally, our approach is generalizable to other disease areas for which reliable disease-specific data are available, making it a potentially important computational platform for both drug target identification and prioritizing targets for drug repurposing efforts.

MATERIALS AND METHODS

High throughput data acquisition and integration

We collected transcriptomics data from the GEO⁶⁹ database and proteomics data³¹. A total of 121 transcriptomics^{22–30} and 20 proteomics³¹ samples relevant to the CD4⁺ T cells were selected (Supplementary Data 1). Transcriptomics data analysis was performed using the *affy*⁷⁰ and *limma*⁷¹ R packages. Because we aimed to characterize gene activities instead of gene expression levels, the processed transcriptomics data were discretized (active = 1; inactive = 0) and samples for each cell type were combined. Genes expressed in more than 50% of the samples in which the probe was present were considered as active (see Supplementary Methods 2). Similarly, proteins expressed in more than 50% of samples in the proteomics dataset were considered as active. In the proteomics datasets, protein IDs were mapped to gene IDs.

Next, we integrated activities from transcriptomics and proteomics datasets. First, biological entities that overlapped in both types of data were selected as high-confidence. Second, we found that some genes were expressed in the majority of transcriptomics datasets, but expressed in less than 50% samples of proteomics data. Similarly, some proteins were identified within groups of highly abundant proteins in multiple samples in proteomics datasets but expressed in less than 50% samples of transcriptomics datasets. Such non-overlapping genes were selected as moderate-confidence based on consensus in single types of -omics data (Supplementary Methods 2.1.1). Third, moderate-confidence genes exclusively present in the transcriptomics data were added to the overlapping genes if expressed in at least 90% of samples. Fourth, moderate-confidence genes exclusively present in the proteomics dataset were added if their abundance was ranked in the top 25% (fourth quartile) (Supplementary Methods 2; Supplementary Data 10). We used these cutoffs to decrease the false negatives while not selecting false positives by removing genes and proteins that are not expressed in any sample either in transcriptomics or proteomics data.

Cell type-specific genome-scale metabolic model reconstruction

We used the GIMME⁷² method (in COBRA toolbox) to construct the metabolic models of different CD4⁺ T cells (naïve, Th1, Th2, Th17). The inputs for GIMME were the generic human Recon3D³⁵ (as a template) and gene expressions based on integrated multi-omics data. The template Recon3D was modified prior to constructing CD4⁺ T-cell-specific metabolic models. These modifications included gene-protein-reaction (GPR) associations (all genes associated with a reaction written using AND and OR operators), media conditions, and reaction directionality. In the original Recon3D, GPRs used transcript IDs. Because our data included gene IDs, we mapped the transcript IDs to the gene IDs. For naïve and effector cells, different types of media conditions were selected based on nutrient

preference information obtained from the literature (Supplementary Methods 2.1.2). In addition, new reactions involved in the biomass objective function were added, and some reactions were removed as described below (see also Supplementary Methods 2). The transcriptomics and proteomics data have information about genes/proteins instead of transcript variants. To map the data obtained for genes, we updated transcript IDs provided in Recon3D to Entrez gene IDs. A total of 1892 genes were included in the modified Recon3D model. Furthermore, because different CD4⁺ T cells have different nutrient uptake preferences, we used two types of media conditions (one for each naïve and one for all effector T cells), shown in Supplementary Methods 2.1.2.4. For all cell subtypes, in addition to the basal metabolites (freely available, i.e., H₂O, O₂, H, O₂S, CO₂, Pi, H₂O₂, HCO₃, H₂CO₃, and CO), glucose, glutamine, and other amino acids were set as open (but tightly constrained) for uptake. The major difference in media condition was the presence of fatty acids in the naïve model. Furthermore, during the refinement of the CD4⁺ T-cell models, the directionality of some reactions was updated based on the Recon 2.2.05 model⁷³ and the MetaCyc database (Supplementary Methods 2.1.2.5 and 2.2.3). Because of the lack of CD4⁺ T-cell-specific data, the biomass objective function was adopted from the macrophage model iAB-AMØ-1410⁷⁴ and added to the Recon3D.

For each subtype, we constructed three models based on transcriptomics, proteomics, and integrated (transcriptomics and proteomics data) datasets. A comparison of these models is provided in Supplementary Fig. 16 and details can be found in Supplementary Methods 2. The models constructed with integrated data were selected for further analysis. Additionally, to investigate the effect of biomass objective function on constructed models, we built two models using biomass objective functions from (1) Recon3D and (2) iAB-AMØ-1410 models. The reactions in output models generated based on each biomass function were compared. The models based on the two objective functions were not significantly different (Supplementary Fig. 17) with respect to the numbers of reactions. Biomass objective function from iAB-AMØ-1410 consists of few extra precursors that predicted better fluxes through fatty acid pathways. The literature has shown that effector CD4⁺ T cells synthesize fatty acids, whereas naïve CD4⁺ T cells exhibit fatty acid oxidation. We compared the fluxes of models created with objective functions from Recon3D and iAB-AMØ-1410. The models created with biomass objective function adopted from iAB-AMØ-1410 had more reactions carrying non-zero flux in the fatty acid pathways (than the models created with Recon3D biomass objective function). Therefore, models that are constructed based on biomass reaction adopted from iAB-AMØ-1410 were used in subsequent analyses. Models were further reduced by removing the dead-end reactions. Reactions in the models are distributed across different compartments including extracellular, cytoplasm, mitochondria, nucleus, Golgi apparatus, lysosome, and endoplasmic reticulum. The models were investigated to perform basic properties using leak tests, gene deletion, and further refined in an iterative manner. To examine leaks, we simulated the models with all the exchange reactions closed and analyzed all the reactions individually for non-zero flux. If the models were producing metabolites, the mass imbalance was checked and fixed. We used a gene deletion analysis to check if the model was able to predict gene essentiality. Because effector T cells are highly glycolytic, deleting glucose transporters should result in reduced growth. We used this as a reference to check that the model was behaving correctly. Furthermore, we investigated if inhibiting acetyl-CoA carboxylase (ACC1)—which was experimentally observed as essential for CD4⁺ T-cell function—resulted in altered growth. These analyses helped us identify problematic reactions that were corrected based on Recon2.2.05—a manually curated model for mass charge balancing and reaction directionality—and the MetaCyc database. Refined models were then subjected to 460 metabolic tasks that were used with the Recon3D model and included in *Test4HumanFctExt* function in COBRA (Supplementary Data 11). The constructed models were simulated using Flux Balance Analysis (FBA) and Flux Variability Analysis (FVA). The final numbers of metabolites and reactions are presented in Supplementary Table 1. These models were named as TNM1055 (naïve model), T1M1133 (Th1 model), T2M1127 (Th2 model), and T17M1250 (Th17 model). The models encoded in json can be found as Supplementary Data 3–6. They have also been submitted to BioModels database⁷⁵ under accessions MODEL1909260003, MODEL1909260004, MODEL1909260005, MODEL1909260006.

Model validation

Models were validated based on literature knowledge related to active pathways in proliferating and differentiated CD4⁺ T cells. CD4⁺ T-cell-specific metabolic functions were searched in the literature using PubMed⁷⁶. Naïve CD4⁺ T cells tend to have low energy demands and mainly rely on fatty acid β -oxidation, oxidation of pyruvate, and glutamine via the TCA cycle⁷⁷. On the other hand, the high bioenergetics demand in effector cells is met by shifting OXPPOS to glycolysis and fatty acid oxidation to fatty acid synthesis³⁹. Furthermore, similar to cancer cells, proliferating effector CD4⁺ T cells convert lactate from pyruvate by lactate dehydrogenase enzyme³⁹. Thus, we obtained the flux distribution of metabolic pathways under wild-type conditions using Flux Balance Analysis (FBA) and searched the non-zero fluxes through the aforementioned pathways in all the models. Flux maps were created using Escher web application (<https://escher.github.io/#/>)^{78,79}. It has also been observed previously that deficiency in glucose and glutamine impairs CD4⁺ T-cell activation and proliferation^{37,80}. We performed this experiment in silico, whereby we varied the flux through exchange reactions of glucose (EX_glc_D[e]) and glutamine (EX_gln_L[e]) in the models and analyzed the effect on growth rate.

Comparison of essential genes predicted by the models and identified in different cell lines

To predict gene essentiality, we knocked out model genes to predict their effect on the growth rate. This was performed using *singleGeneDeletion* in the COBRA toolbox using the Minimization of Metabolic Adjustment (MoMA) method⁸¹. Because of the unavailability of CD4⁺ T-cell-specific data, predicted essential genes were compared with experimentally identified essential genes in humans from different cell lines. The data for experimentally tested essential and nonessential genes for human were obtained from the OGEE database⁴¹. In this database, the essentiality data for humans was compiled using 18 experiments across various cell lines that include RNAi-based inhibition, CRISPR, and CRISPR-CAS9 systems. To investigate how many model-predicted essential genes are also essential in other cell lines, predicted essential genes were compared with experimentally observed essential and conditionally essential genes reported in the OGEE database. Essential and conditionally essential genes were merged together. Additional validations of models using CD4⁺ T-cell-specific essential genes can be found in Supplementary Methods 3.

Mapping drug targets

The developed models were used to predict potential drug targets for autoimmune diseases in which effector subtypes have been found hyperactive^{82,83}. Therefore, a reasonable drug target should downregulate effector CD4⁺ T cells. Among the metabolic genes of selected models, we first identified targets of existing drugs. The drugs and their annotations including target genes were imported from The Drug Repurposing Hub⁸⁴ in the ConnectivityMap (CMap) database⁸⁵ (see also Supplementary Methods 4). All withdrawn drugs and their annotations were first removed. In this list, the gene symbols of target genes of drugs were converted to Entrez IDs. Next, we searched Entrez IDs from CMap data in the genes of metabolic models. For each mapped gene in the model, the drugs were listed.

Metabolic genes differentially expressed in autoimmune diseases

The lack of reliable data from specific CD4⁺ T-cell subtypes involved in autoimmune disease conditions led us to utilize patients' data (case-control studies) available for autoimmune diseases that were collected from peripheral CD4⁺ T cells. Datasets GSE56649⁸⁶ (rheumatoid arthritis), GSE43591⁸⁷ (multiple sclerosis), and GSE93170⁸⁸ (primary biliary cholangitis) were obtained from the GEO database (see details in Supplementary Methods 5). Raw data files were processed using the *affy* and *limma* packages^{70,71} in Bioconductor/R. The *limma* package was used to identify DEGs between patients and healthy controls. For significant differential expression, selective cutoffs of fold-changes were used with adjusted *P*-values < 0.05. For differentially expressed genes, we used a two-fold cutoff. A cutoff of 1.5-fold was used for datasets where two-fold resulted in a very low number to zero differentially expressed metabolic genes.

Perturbation of metabolism and perturbation effect score (PES)

In metabolic models, the knockout of genes that are targets of existing drugs was performed in the COBRA toolbox using MoMA⁸¹ (Supplementary Methods 6). For each knockout, we investigated the change in fluxes regulated by DEGs in diseases. The change in fluxes was computed using flux ratios of perturbed flux/WT flux, and all fluxes that are affected by each perturbation were calculated. We counted fluxes regulated by upregulated genes that are decreased or increased after perturbation (UpDec and UpInc) as well as fluxes regulated by downregulated genes that are decreased or increased after perturbation (DownDec and DownInc). The total number of fluxes for each perturbation also include upregulated genes that were unchanged after perturbation (UpUnc) as well as downregulated genes that were unchanged after perturbation (DownUnc) (see also Supplementary Methods 7). For each perturbed gene, a perturbation effect score (PES) was calculated as:

$$PES = \frac{(UpDec - UpInc)}{(UpDec + UpInc + UpUnc)} + \frac{(DownInc - DownDec)}{(DownInc + DownDec + DownUnc)} \quad (1)$$

Next, for each disease and model combination, the ranks of PES were computed. The gene with the highest PES obtained the top rank and the one with the minimum PES obtained the lowest rank. For each disease, we prioritized drug targets by utilizing their ranks across all models. The PES ranks in each model were first transformed into Z-score as:

$$Z - score = \frac{(x - \mu)}{\sigma} \quad (2)$$

where *x* is a PES rank, μ is the mean of PES ranks in a model for one disease, σ is the standard deviation of PES ranks obtained by a model for one disease. For each disease type and each gene, Z-scores across four models were summed up to calculate an aggregated Z-score. Genes were ranked based on minimum to maximum aggregate Z-scores (Supplementary Methods 8).

Pathway enrichment analysis

For biological processes enrichment analysis, we used DAVID V6.8⁸⁹, and STRING database⁹⁰ together with Gene Ontology biological processes⁹¹, KEGG pathways⁹², and Reactome pathways⁹³. A cutoff of 5%^{94,95} False Discovery Rate (FDR) and *P*-value < 0.05 were used for significant enrichment.

The pathway maps used in Fig. 6 were generated with yED graph editor software. The ChEMBL IDs⁹⁶ of drug targets can be found in Supplementary Table 2.

Experimental validation

We used frozen vials of peripheral blood mononuclear (PBMCs) (IXCells Biotechnologies) from healthy donors. CD4⁺ were purified by negative selection using magnetic human CD4⁺ T cells nanobeads (MojoSort, Biolegend) according to the manufacturer's protocol. For cell activation, anti-CD3 (clone OKT3, Biolegend) was coated on plates at 4 μ g/ml overnight in PBS at 4 °C. Cells were then cultured in X-Vivo media (Lonza) supplemented with 2 μ g/ml of anti-CD28 (clone CD28.2, Biolegend) and with 10 ng/ml of recombinant IL-2 (Peprotech) for 7 days. Half of the media was renewed every 2–3 days by adding fresh media supplemented with 2 μ g/ml of anti-CD28 and 10 ng/ml IL-2.

We purchased alpha-difluoromethylornithine (DFMO) and eicosapentaenoic Acid (EPA) from Cayman Chemical. DFMO was resuspended in water at 50 mM while EPA was already resuspended in ethanol at 826 mM. Perhexiline, Entacapone, and Fluorouracil were obtained from Tocris and dissolved in DMSO to make a stock solution at 12 mM, 200 mM, and 198 mM, respectively. For drug treatment, CD4⁺ T cells were seeded at 50,000 cells in 96 round bottom wells in culture media supplemented with anti-CD3, anti-CD28, and IL-2. Before incubation with CD4⁺ T cells, drugs were diluted in culture media with concentration ranging from 1 μ M to 1000 μ M and incubated for 48 h or 72 h.

We assessed T-cell proliferation using the TACS MTT proliferation assay (R&D Systems). Briefly, a tetrazolium salt solution (10 μ l) was added to each well, and the plate was incubated at 37 °C for 4 h. After incubation, 100 μ l of stop solution was added to each well and incubated overnight before absorbance measurement. Cell proliferation was read at 48 h and 72 h post drug treatment. The absorbance was measured at 570 nm using the BioTek

microplate reader instrument (BioSPX). We corrected cell absorbance readings using cells treated with DMSO or the media controls.

The CD4⁺ T-cell proliferation upon drug treatment was analyzed statistically with a paired *t*-test, one-tailed for four independent experiments. All data are presented as mean plus or minus standard error of the mean (SEM) and analyzed using GraphPad Prism software. The fold change of cell proliferation-cultured was calculated using untreated cells as 1.

Reporting summary

Further information on research design is available in the Nature Research Reporting Summary linked to this article.

DATA AVAILABILITY

The models (TNM1055, T1M1133, T2M1127, and T17M1250) generated in this study are available as json files in the Supplementary Data 3,4,5, and 6 and can also be accessed from the BioModels database under accession MODEL1909260003, MODEL1909260004, MODEL1909260005, MODEL1909260006. The publicly available transcriptomics datasets analyzed in this study are available in GEO (<https://www.ncbi.nlm.nih.gov/geo/>) under accession numbers: GSE2770, GSE22045, GSE22886, GSE24634, GSE30664, GSE42569, GSE43005, GSE43769, GSE50175, GSE60679, GSE56649, GSE43591, and GSE93170. The proteomics dataset used in this study is available in Supplementary Information of Rieckmann et al.³¹.

CODE AVAILABILITY

The scripts used in this pipeline are available on reasonable request.

Received: 17 January 2020; Accepted: 8 December 2020;

Published online: 22 January 2021

REFERENCES

- Zhu, J. & Paul, W. E. CD4 T cells: fates, functions, and faults. *Blood* **112**, 1557–1569 (2008).
- Michalek, R. D. et al. Cutting edge: distinct glycolytic and lipid oxidative metabolic programs are essential for effector and regulatory CD4⁺ T cell subsets. *J. Immunol.* **186**, 3299–3303 (2011).
- Chang, C.-H. et al. Posttranscriptional control of T cell effector function by aerobic glycolysis. *Cell* **153**, 1239–1251 (2013).
- Granados, H. M. et al. Programmed cell death-1, PD-1, is dysregulated in T cells from children with new onset type 1 diabetes. *PLOS ONE* **12**, e0183887 (2017).
- Lü, S. et al. PKM2-dependent metabolic reprogramming in CD4⁺ T cells is crucial for hyperhomocysteinemia-accelerated atherosclerosis. *J. Mol. Med.* **96**, 585–600 (2018).
- Le Bourgeois, T. et al. Targeting T cell metabolism for improvement of cancer immunotherapy. *Front. Oncol.* **8**, 237 (2018).
- Yang, Z., Fujii, H., Mohan, S. V., Goronzy, J. J. & Weyand, C. M. Phosphofructokinase deficiency impairs ATP generation, autophagy, and redox balance in rheumatoid arthritis T cells. *J. Exp. Med.* **210**, 2119–2134 (2013).
- Okano, T., Saegusa, J., Takahashi, S., Ueda, Y. & Morinobu, A. Immunometabolism in rheumatoid arthritis. *Immunol. Med.* **41**, 89–97 (2018).
- Gerriets, V. A. et al. Metabolic programming and PDHK1 control CD4⁺ T cell subsets and inflammation. *J. Clin. Invest.* **125**, 194–207 (2015).
- Jones, D. E. T-cell autoimmunity in primary biliary cirrhosis. *Clin. Sci.* **91**, 551–558 (1996).
- Yin, Y. et al. Normalization of CD4⁺ T cell metabolism reverses lupus. *Sci. Transl. Med.* **7**, 274ra18 (2015).
- Yang, Z., Matteson, E. L., Goronzy, J. J. & Weyand, C. M. T-cell metabolism in autoimmune disease. *Arthritis Res. Ther.* **17**, 29 (2015).
- Hedegaard, C. J. et al. T helper cell type 1 (Th1), Th2 and Th17 responses to myelin basic protein and disease activity in multiple sclerosis. *Immunology* **125**, 161–169 (2008).
- Yin, Y. et al. Glucose oxidation is critical for CD4⁺ T cell activation in a mouse model of systemic lupus erythematosus. *J. Immunol.* **196**, 80–90 (2016).
- Pushpakom, S. et al. Drug repurposing: progress, challenges and recommendations. *Nat. Rev. Drug Discov.* **18**, 41–58 (2019).
- Soria-Castro, R. et al. Exploring the drug repurposing versatility of valproic acid as a multifunctional regulator of innate and adaptive immune cells. *J. Immunol. Res.* **2019**, 9678098 (2019).
- Bettencourt, I. A. & Powell, J. D. Targeting metabolism as a novel therapeutic approach to autoimmunity, inflammation, and transplantation. *J. Immunol.* **198**, 999–1005 (2017).
- Puniya, B. L., Kulshreshtha, D., Verma, S. P., Kumar, S. & Ramachandran, S. Integrated gene co-expression network analysis in the growth phase of *Mycobacterium tuberculosis* reveals new potential drug targets. *Mol. Biosyst.* **9**, 2798–2815 (2013).
- Puniya, B. L., Allen, L., Hochfelder, C., Majumder, M. & Helikar, T. Systems perturbation analysis of a large-scale signal transduction model reveals potentially influential candidates for cancer therapeutics. *Front. Bioeng. Biotechnol.* **4**, 10 (2016).
- Puniya, B. L., Kulshreshtha, D., Mittal, I., Mobeen, A. & Ramachandran, S. Integration of metabolic modeling with gene co-expression reveals transcriptionally programmed reactions explaining robustness in *Mycobacterium tuberculosis*. *Sci. Rep.* **6**, 23440 (2016).
- Geyer, P. E., Holdt, L. M., Teupser, D. & Mann, M. Revisiting biomarker discovery by plasma proteomics. *Mol. Syst. Biol.* **13**, 942 (2017).
- Lund, R., Aittokallio, T., Nevalainen, O. & Laheesmaa, R. Identification of novel genes regulated by IL-12, IL-4, or TGF-beta during the early polarization of CD4⁺ lymphocytes. *J. Immunol.* **171**, 5328–5336 (2003).
- Abbas, A. R. et al. Immune response in silico (IRIS): immune-specific genes identified from a compendium of microarray expression data. *Genes Immun.* **6**, 319–331 (2005).
- Zhang, H. et al. Profiling of human CD4⁺ T-cell subsets identifies the TH2-specific noncoding RNA GATA3-AS1. *J. Allergy Clin. Immunol.* **132**, 1005–1008 (2013).
- Bernier, A. et al. Transcriptional profiling reveals molecular signatures associated with HIV permissiveness in Th1Th17 cells and identifies peroxisome proliferator-activated receptor gamma as an intrinsic negative regulator of viral replication. *Retrovirology* **10**, 160 (2013).
- Kleinewietfeld, M. et al. Sodium chloride drives autoimmune disease by the induction of pathogenic TH17 cells. *Nature* **496**, 518–522 (2013).
- Gustafsson, M. et al. A validated gene regulatory network and GWAS identifies early regulators of T cell-associated diseases. *Sci. Transl. Med.* **7**, 313ra178 (2015).
- Prots, I., Skapenko, A., Lipsky, P. E. & Schulze-Koops, H. Analysis of the transcriptional program of developing induced regulatory T cells. *PLoS One* **6**, e16913 (2011).
- Bonacci, B. et al. Requirements for growth and IL-10 expression of highly purified human T regulatory cells. *J. Clin. Immunol.* **32**, 1118–1128 (2012).
- Santarasci, V. et al. Rarity of human T helper 17 cells is due to retinoic acid orphan receptor-dependent mechanisms that limit their expansion. *Immunity* **36**, 201–214 (2012).
- Rieckmann, J. C. et al. Social network architecture of human immune cells unveiled by quantitative proteomics. *Nat. Immunol.* **18**, 583–593 (2017).
- Mao, L. et al. A constraint-based modelling approach to metabolic dysfunction in Parkinson's disease. *Comput. Struct. Biotechnol. J.* **13**, 484–491 (2015).
- C, G., Gb, K., Wj, K., Hu, K. & Sy, L. Current status and applications of genome-scale metabolic models. *Genome Biol.* **20**, 121–121 (2019).
- Han, F., Li, G., Dai, S. & Huang, J. Genome-wide metabolic model to improve understanding of CD4(+) T cell metabolism, immunometabolism and application in drug design. *Mol. Biosyst.* **12**, 431–443 (2016).
- Brunk, E. et al. Recon3D enables a three-dimensional view of gene variation in human metabolism. *Nat. Biotechnol.* **36**, 272–281 (2018).
- Thiele, I. et al. A community-driven global reconstruction of human metabolism. *Nat. Biotechnol.* **31**, 419–425 (2013).
- Macintyre, A. N. et al. The glucose transporter Glut1 is selectively essential for CD4 T cell activation and effector function. *Cell Metab.* **20**, 61–72 (2014).
- Patel, C. H., Leone, R. D., Horton, M. R. & Powell, J. D. Targeting metabolism to regulate immune responses in autoimmunity and cancer. *Nat. Rev. Drug Discov.* **18**, 669–688 (2019).
- Almeida, L., Lochner, M., Berod, L. & Sparwasser, T. Metabolic pathways in T cell activation and lineage differentiation. *Semin. Immunol.* **28**, 514–524 (2016).
- Buck, M. D., O'Sullivan, D. & Pearce, E. L. T cell metabolism drives immunity. *J. Exp. Med.* **212**, 1345–1360 (2015).
- Chen, W.-H., Lu, G., Chen, X., Zhao, X.-M. & Bork, P. OGEE v2: an update of the online gene essentiality database with special focus on differentially essential genes in human cancer cell lines. *Nucleic Acids Res.* **45**, D940–D944 (2017).
- Tian, J., Yong, J., Dang, H. & Kaufman, D. L. Oral GABA treatment downregulates inflammatory responses in a mouse model of rheumatoid arthritis. *Autoimmunity* **44**, 465–470 (2011).
- Breedveld, F. C. & Dayer, J. M. Leflunomide: mode of action in the treatment of rheumatoid arthritis. *Ann. Rheum. Dis.* **59**, 841–849 (2000).

44. Lian, G. et al. Glutathione de novo synthesis but not recycling process coordinates with glutamine catabolism to control redox homeostasis and directs murine T cell differentiation. *eLife* **7**, e36158 (2018).
45. Ashtari, F. & Savoj, M. R. Effects of low dose methotrexate on relapsing-remitting multiple sclerosis in comparison to interferon β -1 α : A randomized controlled trial. *J. Res. Med. Sci.* **16**, 457–462 (2011).
46. Barberis, M., Helikar, T. & Verbruggen, P. Simulation of stimulation: cytokine dosage and cell cycle crosstalk driving timing-dependent T cell differentiation. *Front. Physiol.* **9**, 879 (2018).
47. Kumar, P. & Banik, S. Pharmacotherapy options in rheumatoid arthritis. *Clin. Med. Insights* **6**, 35–43 (2013).
48. Li, E. K., Tam, L.-S. & Tomlinson, B. Leflunomide in the treatment of rheumatoid arthritis. *Clin. Ther.* **26**, 447–459 (2004).
49. Schweitzer, B. I., Dicker, A. P. & Bertino, J. R. Dihydrofolate reductase as a therapeutic target. *FASEB J.* **4**, 2441–2452 (1990).
50. Wishart, D. S. et al. DrugBank 5.0: a major update to the DrugBank database for 2018. *Nucleic Acids Res.* **46**, D1074–D1082 (2018).
51. Bhandage, A. K. et al. GABA regulates release of inflammatory cytokines from peripheral blood mononuclear cells and CD4⁺ T cells and is immunosuppressive in type 1 diabetes. *EBioMedicine* **30**, 283–294 (2018).
52. Mendu, S. K., Bhandage, A., Jin, Z. & Birnir, B. Different subtypes of GABA-A receptors are expressed in human, mouse and rat T lymphocytes. *PLoS One* **7**, e42959 (2012).
53. Jin, Z., Mendu, S. K. & Birnir, B. GABA is an effective immunomodulatory molecule. *Amino Acids* **45**, 87–94 (2013).
54. Safran, M. et al. GeneCards version 3: the human gene integrator. *Database* **2010**, baq020 (2010).
55. The UniProt Consortium. UniProt: the universal protein knowledgebase. *Nucleic Acids Res.* **45**, D158–D169 (2017).
56. Bruzzone, S. et al. Catastrophic NAD⁺ depletion in activated T lymphocytes through Namp1 inhibition reduces demyelination and disability in EAE. *PLoS One* **4**, e7897 (2009).
57. Roulston, A. & Shore, G. C. New strategies to maximize therapeutic opportunities for NAMPT inhibitors in oncology. *Mol. Cell. Oncol.* **3**, e1052180 (2016).
58. Reisdorf, W. C. et al. Preclinical evaluation of EPHX2 inhibition as a novel treatment for inflammatory bowel disease. *PLoS One* **14**, e0215033 (2019).
59. Alves-Filho, J. C. & Pálsson-McDermott, E. M. Pyruvate kinase M2: a potential target for regulating inflammation. *Front. Immunol.* **7**, 145 (2016).
60. Bietz, A., Zhu, H., Xue, M. & Xu, C. Cholesterol metabolism in T cells. *Front. Immunol.* **8**, 1664 (2017).
61. Flinn, A. M. & Genney, A. R. Adenosine deaminase deficiency: a review. *Orphanet J. Rare Dis.* **13**, 65 (2018).
62. Case, A. J. et al. Elevated mitochondrial superoxide disrupts normal T cell development, impairing adaptive immune responses to an influenza challenge. *Free Radic. Biol. Med.* **50**, 448–458 (2011).
63. Wang, R. & Green, D. R. Metabolic reprogramming and metabolic dependency in T cells. *Immunol. Rev.* **249**, 14–26 (2012).
64. Calabrese, E. J. & Mattson, M. P. How does hormesis impact biology, toxicology, and medicine? *NPJ Aging Mech. Dis.* **3**, 1–8 (2017).
65. Slack, M., Wang, T. & Wang, R. T cell metabolic reprogramming and plasticity. *Mol. Immunol.* **68**, 507–512 (2015).
66. Puniya, B. L. et al. A mechanistic computational model reveals that plasticity of CD4⁺ T cell differentiation is a function of cytokine composition and dosage. *Front. Physiol.* **9**, 878 (2018).
67. Carbo, A. et al. Systems modeling of molecular mechanisms controlling cytokine-driven CD4⁺ T cell differentiation and phenotype plasticity. *PLoS Comput. Biol.* **9**, e1003027 (2013).
68. Jerby, L. & Ruppén, E. Predicting drug targets and biomarkers of cancer via genome-scale metabolic modeling. *Clin. Cancer Res.* **18**, 5572–5584 (2012).
69. Barrett, T. et al. NCBI GEO: archive for functional genomics data sets—update. *Nucleic Acids Res.* **41**, D991–D995 (2013).
70. Gautier, L., Cope, L., Bolstad, B. M. & Irizarry, R. A. affy—analysis of Affymetrix GeneChip data at the probe level. *Bioinformatics* **20**, 307–315 (2004).
71. Ritchie, M. E. et al. Limma powers differential expression analyses for RNA-seq and microarray studies. *Nucleic Acids Res.* **43**, e47 (2015).
72. Becker, S. A. & Pálsson, B. O. Context-specific metabolic networks are consistent with experiments. *PLoS Comput. Biol.* **4**, e1000082 (2008).
73. Swainston, N. et al. Recon 2.2: from reconstruction to model of human metabolism. *Metabolomics* **12**, 109 (2016).
74. Bordbar, A., Lewis, N. E., Schellenberger, J., Pálsson, B. Ø. & Jamshidi, N. Insight into human alveolar macrophage and *M. tuberculosis* interactions via metabolic reconstructions. *Mol. Syst. Biol.* **6**, 422 (2010).
75. Chelliah, V. et al. BioModels: ten-year anniversary. *Nucleic Acids Res.* **43**, D542–D548 (2015).
76. Sayers, E. W. et al. Database resources of the National Center for Biotechnology Information. *Nucleic Acids Res.* **47**, D23–D28 (2019).
77. Patsoukis, N. et al. The role of metabolic reprogramming in T cell fate and function. *Curr. Trends Immunol.* **17**, 1–12 (2016).
78. Rowe, E., Pálsson, B. O. & King, Z. A. Escher-FBA: a web application for interactive flux balance analysis. *BMC Syst. Biol.* **12**, 84 (2018).
79. King, Z. A. et al. Escher: a web application for building, sharing, and embedding data-rich visualizations of biological pathways. *PLoS Comput. Biol.* **11**, e1004321 (2015).
80. Ren, W. et al. Amino-acid transporters in T-cell activation and differentiation. *Cell Death Dis.* **8**, e2757 (2017).
81. Segrè, D., Vitkup, D. & Church, G. M. Analysis of optimality in natural and perturbed metabolic networks. *Proc. Natl Acad. Sci. U.S.A.* **99**, 15112–15117 (2002).
82. Ivanova, E. A. & Orekhov, A. N. T helper lymphocyte subsets and plasticity in autoimmunity and cancer: an overview. *BioMed. Res. Int.* **2015**, 327470 (2015).
83. Hoyer, K. K., Kuswanto, W. F., Gallo, E. & Abbas, A. K. Distinct roles of helper T-cell subsets in a systemic autoimmune disease. *Blood* **113**, 389–395 (2009).
84. Corsello, S. M. et al. The drug repurposing hub: a next-generation drug library and information resource. *Nat. Med.* **23**, 405–408 (2017).
85. Subramanian, A. et al. A next generation connectivity map: L1000 platform and the first 1,000,000 profiles. *Cell* **171**, 1437–1452.e17 (2017).
86. Ye, H. et al. CD4 T-cell transcriptome analysis reveals aberrant regulation of STAT3 and Wnt signaling pathways in rheumatoid arthritis: evidence from a case-control study. *Arthritis Res. Ther.* **17**, 76 (2015).
87. Jernäs, M. et al. MicroRNA regulate immune pathways in T-cells in multiple sclerosis (MS). *BMC Immunol.* **14**, 32 (2013).
88. Nakagawa, R. et al. miR-425 regulates inflammatory cytokine production in CD4⁺ T cells via N-Ras upregulation in primary biliary cholangitis. *J. Hepatol.* **66**, 1223–1230 (2017).
89. Huang, D. W., Sherman, B. T. & Lempicki, R. A. Systematic and integrative analysis of large gene lists using DAVID bioinformatics resources. *Nat. Protoc.* **4**, 44–57 (2009).
90. Szklarczyk, D. et al. The STRING database in 2017: quality-controlled protein-protein association networks, made broadly accessible. *Nucleic Acids Res.* **45**, D362–D368 (2017).
91. The Gene Ontology Consortium. The gene ontology resource: 20 years and still going strong. *Nucleic Acids Res.* **47**, D330–D338 (2019).
92. Kanehisa, M., Sato, Y., Kawashima, M., Furumichi, M. & Tanabe, M. KEGG as a reference resource for gene and protein annotation. *Nucleic Acids Res.* **44**, D457–D462 (2016).
93. Fabregat, A. et al. The reactome pathway knowledgebase. *Nucleic Acids Res.* **46**, D649–D655 (2018).
94. Boyle, E. I. et al. GO::TermFinder—open source software for accessing gene ontology information and finding significantly enriched gene ontology terms associated with a list of genes. *Bioinformatics* **20**, 3710–3715 (2004).
95. Reimand, J. et al. Pathway enrichment analysis and visualization of omics data using g:Profiler, GSEA, Cytoscape and EnrichmentMap. *Nat. Protoc.* **14**, 482–517 (2019).
96. Gaulton, A. et al. The ChEMBL database in 2017. *Nucleic Acids Res.* **45**, D945–D954 (2017).
97. Herring, T. A., Cuppett, S. L. & Zempleni, J. Genomic implications of H₂O₂ (2) for cell proliferation and growth of Caco-2 cells. *Dig. Dis. Sci.* **52**, 3005–3015 (2007).
98. Rongvaux, A. et al. Nicotinamide phosphoribosyl transferase/pre-B cell colony-enhancing factor/visfatin is required for lymphocyte development and cellular resistance to genotoxic stress. *J. Immunol.* **181**, 4685–4695 (2008).
99. Marks, R. E. et al. Farnesyltransferase inhibitors inhibit T-cell cytokine production at the posttranscriptional level. *Blood* **110**, 1982–1988 (2007).
100. Surls, J. et al. Increased membrane cholesterol in lymphocytes diverts T-cells toward an inflammatory response. *PLoS One* **7**, e38733 (2012).
101. Ando, T. et al. Transduction with the antioxidant enzyme catalase protects human T cells against oxidative stress. *J. Immunol.* **181**, 8382–8390 (2008).
102. MacPherson, S. et al. STAT3 regulation of citrate synthase is essential during the initiation of lymphocyte cell growth. *Cell Rep.* **19**, 910–918 (2017).
103. Palmer, A. M. Teriflunomide an inhibitor of dihydroorotate dehydrogenase for the potential oral treatment of multiple sclerosis. *Curr. Opin. Investig. Drugs* **11**, 1313–1323 (2010).
104. Xu, T. & Ding, S. Methods of treating disease by metabolic control of T-cell differentiation. US Patent US20190022142A1 (2019).
105. Arefieva, T. I., Filatova, A. Y., Potekhina, A. V. & Shchinova, A. M. Immunotropic effects and proposed mechanism of action for 3-hydroxy-3-methylglutaryl-coenzyme A reductase inhibitors (statins). *Biochem. Biokhimiya* **83**, 874–889 (2018).
106. Young, K. E., Flaherty, S., Woodman, K. M., Sharma-Walia, N. & Reynolds, J. M. Fatty acid synthase regulates the pathogenicity of Th17 cells. *J. Leukoc. Biol.* **102**, 1229–1235 (2017).

107. Metzler, B., Gfeller, P. & Guinet, E. Restricting glutamine or glutamine-dependent purine and pyrimidine syntheses promotes human T cells with high FOXP3 expression and regulatory properties. *J. Immunol.* **196**, 3618–3630 (2016).
108. Bantia, S. & Kilpatrick, J. M. Purine nucleoside phosphorylase inhibitors in T-cell malignancies. *Curr. Opin. Drug Discov. Devel.* **7**, 243–247 (2004).
109. Mathur, D., López-Rodas, G., Casanova, B. & Marti, M. B. Perturbed glucose metabolism: insights into multiple sclerosis pathogenesis. *Front. Neurol.* **5**, 250 (2014).
110. Antonioli, L. et al. Adenosine deaminase in the modulation of immune system and its potential as a novel target for treatment of inflammatory disorders. *Curr. Drug Targets* **13**, 842–862 (2012).
111. Muri, J. et al. The thioredoxin-1 system is essential for fueling DNA synthesis during T-cell metabolic reprogramming and proliferation. *Nat. Commun.* **9**, 1851 (2018).
112. Osinalde, N. et al. Nuclear phosphoproteomic screen uncovers ACLY as mediator of IL-2-induced proliferation of CD4⁺ T lymphocytes. *Mol. Cell. Proteom. MCP* **15**, 2076–2092 (2016).

ACKNOWLEDGEMENTS

This work was supported by NIH grant 1R35GM119770-04 to T.H. and by the Systems Biology Grant of the University of Surrey to M.B. The corresponding author M.B. can also be contacted at matteo@barberislab.com. The authors thank aSciStance Ltd. for their scientific advice and editing services.

AUTHOR CONTRIBUTIONS

T.H. and B.L.P. conceived the study. B.L.P., M.B., and T.H. designed the study. B.L.P., M.B., and T.H. defined the pipeline to integrate -omics data, and B.L.P. implemented the pipeline. B.L.P. and B.L. performed literature mining. B.L.P., B.L., R.M., A.C., and S.J.B. collected the data. B.L.P., B.L., R.M., and A.C. constructed the models. A.R.S. performed refinement of the constructed models. B.L.P., B.L., R.M., A.C., S.J.B., M.B., and T.H. analyzed the data. R.A. performed the experimental work and analyzed the experimental results. B.L.P., M.B., and T.H. wrote the manuscript. M.B. and T.H. supervised the study.

COMPETING INTERESTS

The authors declare no competing interests.

ADDITIONAL INFORMATION

Supplementary information is available for this paper at <https://doi.org/10.1038/s41540-020-00165-3>.

Correspondence and requests for materials should be addressed to M.B. or T.H.

Reprints and permission information is available at <http://www.nature.com/reprints>

Publisher's note Springer Nature remains neutral with regard to jurisdictional claims in published maps and institutional affiliations.



Open Access This article is licensed under a Creative Commons Attribution 4.0 International License, which permits use, sharing, adaptation, distribution and reproduction in any medium or format, as long as you give appropriate credit to the original author(s) and the source, provide a link to the Creative Commons license, and indicate if changes were made. The images or other third party material in this article are included in the article's Creative Commons license, unless indicated otherwise in a credit line to the material. If material is not included in the article's Creative Commons license and your intended use is not permitted by statutory regulation or exceeds the permitted use, you will need to obtain permission directly from the copyright holder. To view a copy of this license, visit <http://creativecommons.org/licenses/by/4.0/>.

© The Author(s) 2021